Instructional materials that control cellular activity through synthetic Notch receptors

Joanne C. Lee [a], Hannah J. Brien [a], Bonnie L. Walton [a], Zachary M. Eidman [a], Satoshi Toda [b], Wendell A. Lim [c],[**],[1], Jonathan M. Brunger [a],[d],[*],[1]

[a] Department of Biomedical Engineering, Vanderbilt University, Nashville, TN, 37212, USA
[b] WPI Nano Life Science Institute (NanoLSI), Kanazawa University, Kanazawa, Ishikawa, Japan
[c] Cell Design Institute and Department of Cellular and Molecular Pharmacology, University of California, San Francisco, San Francisco, CA, 94158, USA
[d] Center for Stem Cell Biology, Vanderbilt University, Nashville, TN, 37212, USA

ARTICLE INFO

ABSTRACT

The field of regenerative engineering relies primarily on the dual technical platforms of cell selection/conditioning and biomaterial fabrication to support directed cell differentiation. As the field has matured, an appreciation for the influence of biomaterials on cell behaviors has resulted in engineered matrices that meet biomechanical and biochemical demands of target pathologies. Yet, despite advances in methods to produce designer matrices, regenerative engineers remain unable to reliably orchestrate behaviors of therapeutic cells *in situ*. Here, we present a platform named MATRIX whereby cellular responses to biomaterials can be custom defined by combining engineered materials with cells expressing cognate synthetic biology control modules. Such privileged channels of material-to-cell communication can activate synthetic Notch receptors and govern activities as diverse as transcriptome engineering, inflammation attenuation, and pluripotent stem cell differentiation, all in response to materials decorated with otherwise bioinert ligands. Further, we show that engineered cellular behaviors are confined to programmed biomaterial surfaces, highlighting the potential to use this platform to spatially organize cellular responses to bulk, soluble factors. This integrated approach of co-engineering cells and biomaterials for orthogonal interactions opens new avenues for reproducible control of cell-based therapies and tissue replacements.

1. Introduction

Regenerative engineers regard biomaterials as critical for restoring tissue function. In fact, biomaterial scaffolds and cell delivery vehicles serve as one of the main cogs in the tissue engineering gearbox [1], along with cell sourcing and methods for dictating cell phenotype [2,3]. Engineered biomaterials are leveraged as more than simple physical substrata for encapsulating cells or for supporting neomatrix production [4]; instead, modern biomaterials are designed to meet the demands of specific systems-level needs, where the system is defined by the biomechanical, biochemical, and spatial demands of the relevant pathology as well as the complex relationship between cells and their fabricated and biologic microenvironment [5–7]. To serve regenerative engineering needs, materials have been produced with tuned elasticity [8–12], topography [13–18], and pore size [19–21]: these parameters have been shown to influence self-renewal, differentiation, and self-organization of multicellular assemblies [22–27]. Synthetic matrices have been programmed to incorporate native ligands to encourage maintenance of encapsulated cell fate [28] and to encourage synthesis of local tissues [29], or to sequester pro-inflammatory factors [30]. Furthermore, owing in part to advances in "click" chemistry, biomaterial designers have developed means to produce dynamic materials that release bioactive factors in response to triggers such as pH [31,32], temperature [33–35], light [36,37], or the presence of matrix-degrading enzymes in the material microenvironment [38]. However, these dynamic changes unfold over time in an irreversible fashion - once the material releases cargo factors, they lose their ability to further coordinate cell behaviors in response to changes within the

niche [5,39]. Thus, new approaches are needed to complement these advances while enabling sustained, reproducible control of cell behaviors.

Here, we investigate a strategy to co-engineer cells and biomaterial substrata so that a biomaterial provides customized instructions to a cognate engineered cell. Rather than unidirectionally modifying an environment by eluting factors or altering mechanical properties, these materials leverage the computational power of cells to conditionally execute defined functions encoded in artificial gene circuits. We use the synthetic Notch (synNotch) platform [40–43] to engineer cells to respond to selected inputs presented via programmable biomaterials (Fig. 1A). SynNotch is a synthetic receptor platform based on the native Notch signaling channel. By exchanging Notch's (1) extracellular domain with chosen recognition motifs (i.e., single chain variable fragments [scFvs] or nanobodies) and (2) intracellular domain with a synthetic transcription factor such as the tetracycline-controlled trans-activator (tTA), synNotch receptors can produce user-specified sense/-response behaviors. Customized synNotch receptors can bind to chosen ligands to drive expression of any transgene, making it possible to tune defined cellular responses to selected inputs. This facilitates coupling of arbitrarily selected ligands, including orthogonal bioinert factors such as green fluorescent protein (GFP), to desired cell transcriptional programs to support homeostasis and regeneration.

Critically, like the juxtacrine Notch receptor, synNotch requires mechanical strain generated by immobilized ligand for receptor activation, and as such monomeric soluble ligands do not efficiently activate this receptor alone [44]. This feature distinguishes synNotch from other synthetic receptors such as GEARs [45], MESA [46,47], GEMs [48], or TANGO [49,50]. Based on its design, synNotch transgene expression is highly localized to niches decorated with immobilized activators. We have illustrated that conjugation of synNotch ligands directly to microparticles leads to productive regulation of chimeric antigen receptor expression in engineered T cells [51]. Our prior work has also demonstrated a method for converting soluble inputs for synNotch recognition via anchor cells that capture and present ligand to engineered synNotch cells [52]. Here, we build on that work by functionalizing biomaterials with affinity motifs that capture soluble ligands as inputs for synNotch cells. Engineering cells to interface with such programmable biomaterials opens a privileged channel of communication that flexibly offers customized input/output relationships and spatial control over engineered transgene expression. We thus term our platform MATRIX for material activated to regulate inducible expression. In cells ranging from immortalized fibroblasts, primary stem cells, and pluripotent stem cells, we illustrate the versatility of the MATRIX platform for regulating CRISPR-based transcriptome modifiers, modulating inflammatory niches, and mediating stem cell differentiation. These results represent progress toward the design of custom cell-matrix interactions to orchestrate regeneration and repair.

2. Materials and methods

Biomaterial surface functionalization. To prepare GFP capturing biomaterial surfaces, a 12-unit polyethylene glycol (PEG) linker activated with an *N*-hydroxysuccinimide ester (NHS) group on one end and
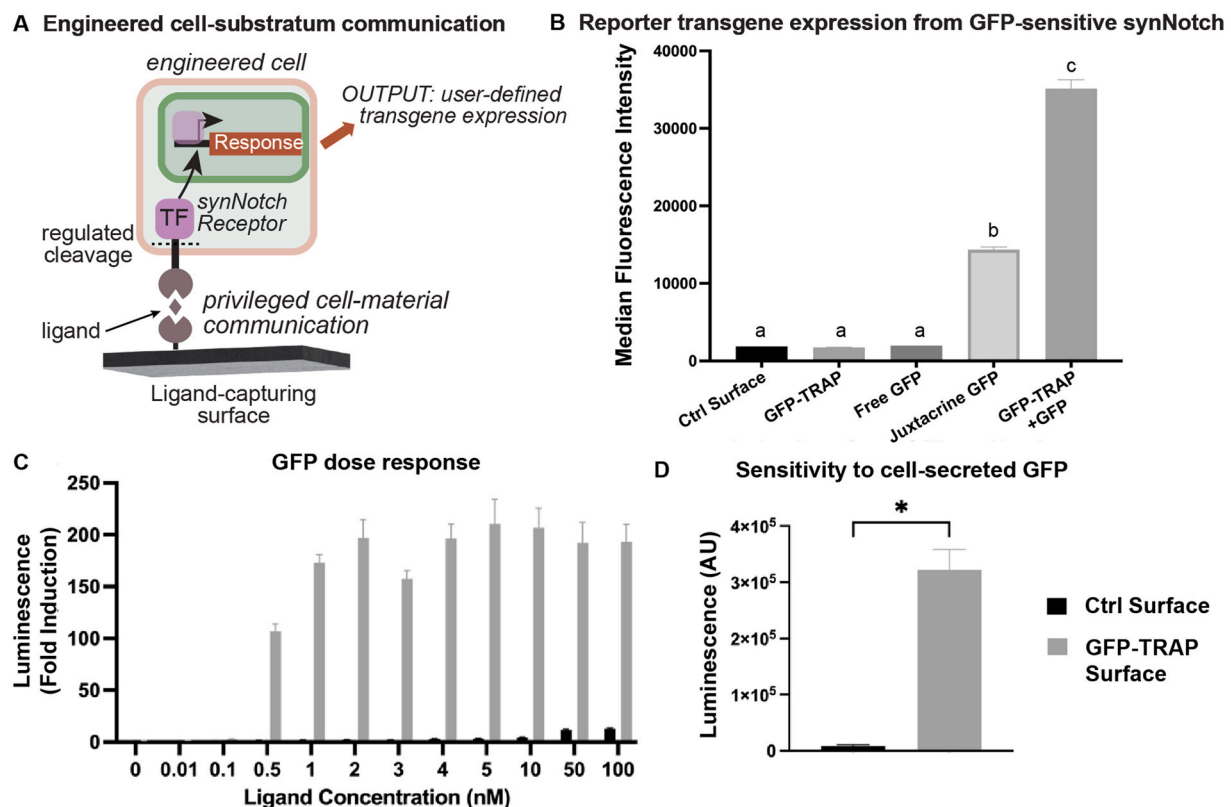

Fig. 1. An integrated cell-biomaterial design platform in which functionalized surfaces instruct custom cellular responses based on synthetic signaling networks. (A) Schematic of the modular synNotch receptor serving as a privileged channel of communication between biomaterial surfaces that capture soluble ligands of interest for presentation to engineered cells. Upon binding of immobilized ligand, proteolytic cleavage of the receptor enables translocation of a transcription factor (TF) to the nucleus to activate target gene expression. (B) Median mCherry fluorescence intensity of engineered GFP-synNotch L929 mouse fibroblast cells activated via indicated modes of ligand presentation. Groups not sharing the same letters are statistically significantly different (one-way ANOVA with Tukey's post-hoc test). (C) Fold change of firefly luminescence across a range of GFP concentrations in GFP-synNotch L929 fibroblasts compared to no GFP control condition. (D) Luminescence values of GFP-synNotch cells co-cultured with GFP-secreting cells with and without the GFP-TRAP surface. (*$p < 0.05$, Welch's *t*-test). In all plots, n = 3 replicates; error bars indicate SEM.

a biotin group on the other (Thermo Scientific) was conjugated to GFP-TRAP (Chromotek) in a reaction containing a 2-fold molar excess of NHS-PEG-biotin. The reaction was allowed to proceed for 1 h at room temperature or overnight at 4 °C and was then quenched by adding 50 mM glycine at pH 2.1, resulting in a stock solution of biotinylated GFP-TRAP at a concentration of 7.19 μM. This solution was then diluted in DPBS to 5.6% v/v, resulting in a solution containing 402 nM conjugate. Then, surfaces of non-tissue culture treated plates were coated with 10 μg/mL streptavidin (Thermo Scientific) in DPBS for a minimum of 1 h at 37 °C. In CasRx experiments, 100 μg/mL streptavidin was used. Streptavidin was aspirated prior to addition of 100 μl of biotinylated GFP-TRAP solution, which was allowed to incubate for 1 h at 37 °C prior to aspiration and use in cell culture experiments.

To produce a substratum compatible with pluripotent stem cell culture, we utilized glycosaminoglycan-binding peptide (GBP, GenScript Express, biotin-Ahx-GKKQRFRHRNRKG) and cRGD (cyclo[Arg-Gly-Asp-D-Phe-Lys(Biotin-PEG-PEG), VIVITIDE), which are derived from vitronectin and fibronectin, respectively, for stem cell adhesion [53,54]. We diluted stock concentrations of GBP and cRGD to 10 μM and 17.85 μM, respectively, in DPBS. An eight micromolar solution of peptides was used to coat culture wells. The stock concentration of 7.19 μM GFP-TRAP was mixed with the GBP and cRGD in a 5:2.2:0.8 (GBP:cRGD:GFP-TRAP) molar ratio. This mixture was used as the GFP-capturing biomaterial substratum. For control substrata without the GFP-capturing motif, GBP and cRGD were combined in a 5:2.15 molar ratio. To construct the biomaterial surface, 10 μg/mL streptavidin was adsorbed onto a non-tissue culture treated 24 well plate for 48 h. Then, the streptavidin was aspirated and either the GFP-capturing peptide combination or the control GBP + cRGD combination was added onto the 24-well plate and allowed to bind to streptavidin for 1–2 h in a cell culture incubator.

Plasmid design and construction. Plasmids were designed with Snapgene and constructed using New England Biolabs HiFi DNA assembly mix. After assembly, plasmids were transformed into NEB5α *E. coli* competent cells (NEB) and plated on an LB + agar with ampicillin supplementation plate for overnight incubation at 37 °C. Appropriate colonies were then picked and cultured in LB with ampicillin supplementation overnight prior to miniprep purification (Qiagen). All plasmids were verified by Sanger sequencing prior to use.

Virus production. Lentivirus was produced by transfecting Lx293 T cells (Clontech) with 2 μg of transfer vector, 1.5 μg of pCMV-dR8.91 packaging vector [55] and 0.6 μg of pMD2.G envelope vector (gift from Didier Trono, Addgene #12259) [56] using Lipofectamine 3000 (Thermo Scientific) following manufacturer's instructions. The following day, medium was exchanged for fresh DMEM-High Glucose supplemented with GlutaMAX and sodium pyruvate as well as 10% heat-inactivated FBS. On each of the following two days, viral supernatant was collected, filtered with a 0.45 μm PVDF filter (CELLTREAT) and pooled for cell transduction or stored short-term (<1 week) at 4 °C or long-term at −80 °C. Lentivirus used to transduce H9 hESCs was produced in OptiMem rather than serum-containing DMEM and concentrated 60-fold in a 100 kDa MWCO filter (EMD Millipore) prior to transduction.

2.1. Cell culture

L929 mouse fibroblasts. Mouse L929 fibroblasts (ATCC# CCL-1) were cultured in DMEM-High Glucose with GlutaMAX (Gibco) and 10% heat-inactivated FBS (Gibco) at 37 °C and 5% carbon dioxide. For experiments, cells were detached with TrypLE Express (Gibco) by incubation at 37 °C for 5 min. Cells were then centrifuged for 5 min at $300 \times g$ and resuspended in L929 culture medium for plating.

Murine mesenchymal stem cells. Bone marrow-derived mesenchymal stem cells from C57BL/6 mice (Cyagen) were cultured in MEM α supplemented with GlutaMAX (Gibco) and 15% FBS in an incubator at 37 °C and 5% carbon dioxide. For subcultivation, cells were rinsed with 1X DPBS (Gibco) for 1 min and then detached with TrypLE by incubation at 37 °C for 5 min. Cells were then centrifuged for 5 min at $300 \times g$ and resuspended in mMSC culture medium for plating.

Human embryonic stem cells. H9 human embryonic stem cells (hESCs, WiCell) were maintained in mTeSR1 or mTeSR Plus medium (STEMCELL Technologies) on Geltrex (Gibco)-coated wells. For routine passaging, cells were detached with ReLeSR (STEMCELL Technologies). To produce a single-cell suspension for flow cytometry or synNotch activation experiments, cells were dissociated with Accutase (Gibco).

Lentiviral transduction. L929 and mMSC cell lines were derived through reverse transduction by passaging and plating with 100% viral media. Media were supplemented with 4 μg/mL of polybrene to facilitate uptake of the lentiviral particles. Viral medium was incubated with target cells overnight and replaced with fresh media the next day. L929 cells were selected in 30 μg/mL puromycin and mMSC cells were selected in 10 μg/mL puromycin where applicable prior to experiments.

For H9 hESC transduction, the concentrate from 2 mL of viral supernatant was resuspended in 2 mL mTesR supplemented with 4 μg/mL of polybrene. The next day, transduction medium was exchanged for fresh mTesR. Cells were selected in 0.6 μg/mL puromycin prior to experiments.

Sleeping Beauty engineering of Ngn2 H9 hESCs. To circumvent silencing of transgenes in differentiating hESCs [57], we relied on the Sleeping Beauty transposase system to produce stable synNotch H9 ESCs for neuronal differentiation experiments [58,59]. Control mCherry alone and Ngn2+mCherry hESC cell lines were derived through transfection with the Sleeping Beauty transposon system using the TransIT-LT1 transfection reagent (Mirus Bio) by transfecting 1 μg Sleeping Beauty transposase plasmid (Addgene 34879, a kind gift from Zsuzsanna Izsvak) [60] and 1 μg transposon (based on Addgene 60495, a kind gift from Eric Kowarz) [61] delivering the synNotch receptor protein as well as the transgene payload. Cells were selected with 0.6 μg/mL puromycin, sorted based on expression of a c-myc-tag epitope appended to the synNotch receptor, and then sub-cultivated prior to use in synNotch activation experiments.

Activation of synNotch cells with biomaterial surfaces. Dissociated synNotch L929 fibroblasts were plated at a density of 18,000 cells/well (56,250 cells/cm^2) on either a control surface of streptavidin only or GFP-TRAP functionalized surfaces. For the juxtacrine condition, synNotch cells were plated at a 1:1 ratio with GFP-ligand sender L929 cells on the control surface. For activation, culture medium was supplemented with indicated concentrations of GFP. Unless otherwise noted, the LaG16 (K_d of 0.7 nM) synNotch receptor was activated with 5 nM recombinant GFP purified from *E. coli* via immobilized metal affinity chromatography. A subset of synNotch cell lines were based on the medium affinity anti-GFP nanobody (LaG17, K_d = 50 nM) [62]. Receptor activation in these experiments involved either 50 nM GFP in the CasRx L929 experiments or 200 nM GFP in H9 hESC reporter activation experiments. After 48 h, firefly luminescence was measured using the BrightGlo luminescence assay (Promega) on a Tecan Infinite M1000 Pro plate reader. Unless otherwise indicated, results are expressed as fold change relative to GFP-free and non-functionalized surface conditions. For flow cytometry measurements, a 24-well non-tissue culture treated plate was used. Cells were gated for the presence of the response element, denoted by a BFP marker, or the synNotch receptor protein marked with a c-myc epitope tag stained with the 9B11 monoclonal antibody conjugated to AlexaFluor647 (Cell Signaling Technologies).

mCherry as a synthetic input. L929 mouse fibroblast cells were transduced with an anti-RFP LaM8 synNotch receptor and a response element with a TRE promoter linked to production of firefly luciferase. Here, we engineered a fusion protein with an mCherry domain and a C-terminal c-myc epitope tag. Magnetic beads displaying anti-c-myc antibodies (Thermo Scientific) served to immobilize a soluble mCherry-myc protein. We seeded a 96-well plate with 18,000 LaM8 synNotch cells per well. Cells were plated with either the mCherry-myc protein only, the anti-myc beads only, or both mCherry-myc and anti-myc

beads. The fusion protein was produced by transfecting an expression plasmid with the mCherry-myc transgene into Lx293 T cells and collecting conditioned media. The medium was then filtered through a 0.45 μm PVDF filter to remove cellular debris. To exchange the bulk conditioned medium for fresh medium, we concentrated the supernatant using a 30 kDa MWCO filter (EMD Millipore) and then resuspended the concentrate in an original volume of fresh culture medium. To activate cells with mCherry-myc ligand, ligand-containing medium was mixed 1:1 with fresh cell culture medium. A final concentration of 0.1 mg/mL of anti-myc beads was added to the cells to capture and immobilize the soluble mCherry-myc protein. After 48 h, firefly luminescence was measured using BrightGlo as indicated above.

Orthogonal activation of synNotch receptors. L929 mouse fibroblast cells were transduced with two synNotch receptors: the LaG16 synNotch receptor with a tTA intracellular domain and the LaM8 synNotch receptor with a Gal4VP64 intracellular domain [40]. They were also transduced with two response elements, one a TRE promoter linked to firefly luciferase, and the other a UAS promoter linked to Renilla luciferase. Cells were plated in culture with or without the combination of GFP, mCherry-myc, and the respective surfaces functionalized to capture each of these ligands. as described above. After 48 h, firefly and Renilla luminescence values were measured with DualGlo (Promega) per manufacturer's instructions.

Sensing cell-secreted ligands. L929 mouse fibroblast cells were transduced with the LaG16 synNotch and an mCherry + firefly luciferase payload. Another population of L929 cells was transduced with a vector driving constitutive secretion of GFP. A 1:1 ratio of 18,000 cells of each type were plated in a 96-well plate either with or without the GFP-TRAP functionalized surface described above. After 48 h, the firefly luminescence was measured using BrightGlo reagent as noted above.

Patterned synthetic signaling via engineered surfaces and synNotch cells. We used a wedge-shaped cell culture insert (Ibidi) divided into quadrants to functionalize different areas of individual wells of a tissue culture treated 12-well plate. For an initial set of experiments using a uniform concentration (5.6% v/v) of GFP-TRAP, surfaces of wells defined by two of the quadrants were functionalized with GFP-TRAP, while surfaces within the other two quadrants and on the outside of the cell culture insert were coated with 5% FBS in DPBS. In a follow-up experiment, we varied the amount of GFP-TRAP used to functionalize surfaces of quadrants defined by the insert using 0%, 1.4%, 5.6%, or 20% v/v GFP-TRAP solutions. After a 1-h incubation, all reagents were aspirated off the plate and the cell culture insert was removed with sterile tweezers. Then, the well was washed with 1 mL DPBS, and 20,000 LaG16-synNotch cells/cm^2 were plated over the entire well surface. GFP at 5 nM was added to the medium. For the cell-secreted version of this experiment, a 1:1 number of cells engineered to secrete GFP were added along with the LaG16 synNotch cells in L929 cell culture medium. Images were taken 48 h after plating. Cells were first stained with 5 μM Draq5 (Thermo Scientific) for 15 min at room temperature to enable visualization of both activated and unactivated cells. Average mCherry pixel intensities were quantified from n = 12 fields of view at 10× magnification using the Fiji mean gray value measurement.

CRISPR-based transcriptome modification regulated via material-mediated artificial signaling. Mouse L929 fibroblasts were engineered with a vector encoding K-cadherin-IRES-mCherry. These cells were engineered to express a LaG17-synNotch receptor driving TRE-inducible expression of CasRx [63]. Finally, these cells were also transduced with vectors encoding CasRx gRNA sequences targeting mCherry. The sequences of mCherry-targeting gRNAs are 5′-CGCCGCCGTCCTCGAAGT TCAT-3′; 5′-GAAGCGCATGAACTCCTTGATG-3′; 5′-TTCATCACGCGCTC CCACTTGA-3′; 5′-ACCTTGAAGCGCATGAACTCCT-3′. Following transduction, cells were sorted based on synNotch receptor, gRNA, and mCherry expression. For synNotch activation experiments, GFP-TRAP functionalized culture surfaces were prepared, and 20,000 cells were added with soluble GFP at a final concentration of 0 or 50 nM. For control conditions,

20,000 cells were added in monolayer on a tissue culture-treated plate.

Mouse mesenchymal stem cell activation with biomaterial surfaces. Mouse mesenchymal stem cells were transduced with the LaG16-synNotch receptor described previously and a response element with a TRE promoter linked to production of secreted alkaline phosphatase (SEAP). A total of 6000 cells/well were plated in a 96-well plate on the GFP-TRAP functionalized surface for each condition supplemented with 0 or 5 nM of GFP and cultured for 96 h. SEAP production for mMSC activation was analyzed using a chemiluminescence assay (Takara Bio), according to the manufacturer's protocol. The samples were then measured on a Tecan Infinite M1000 Pro plate reader.

For experiments investigating the ability of material-mediated suppression of TNF responses, a streptavidin-coated, 96-well non-tissue culture treated plate was functionalized with GFP-TRAP as described above, and 6000 mMSCs were seeded per well. The medium was then supplemented with 5 nM GFP. Two days after plating, the wells were supplemented with medium containing either 0 or 10 ng/mL TNF-α (STEMCELL Technologies). Two days after addition of TNF-α, media were aspirated and saved from each sample for an ELISA, and cells were lysed for quantitative real-time PCR (qRT-PCR). For flow cytometry, cells were plated in a similar fashion in a 24-well non-tissue culture treated plate and harvested via TrypLE dissociation.

Human embryonic stem cell activation via biomaterial surfaces. Engineered H9 hESCs were dissociated with Accutase and plated at 150,000 cells per well of a 24-well plate in 10 μM Y-27632 dihydrochloride, a ROCK inhibitor (Tocris), in mTeSR medium. For conditions with ligand added, 200 nM GFP was supplemented into the medium to activate the LaG17-synNotch. After 24 h, the medium was aspirated and replaced with 5 μM Y-27632 dihydrochloride with and without GFP supplementation in mTeSR. Medium was changed daily until termination of the experiment on day four.

For neuron differentiation experiments, engineered H9 hESCs were cultured on the GBP, cRGD, and GFP-TRAP functionalized surface as described previously. Cells dissociated with Accutase were plated at 50,000 cells/well in a 96-well plate with 10 μM Y-27632 dihydrochloride mTeSR + medium, and 0 or 5 nM GFP. The next day, culture medium was changed to a neurogenic medium, consisting of DMEM F12+GlutaMAX, 1X B-27 with vitamin A (Gibco), and 1X N-2 supplement (Gibco) [64] with 10 μM Y-27632 dihydrochloride. The Y-27632 dihydrochloride concentration was then lowered to 5 μM for the remainder of the experiment. Medium was changed every 24 h for four days prior to preparing cells for immunocytochemistry and mRNA isolation as described below.

2.2. Measurements

Microscopy. All images were taken on a Leica Dmi8 epifluorescent microscope at 10× magnification except for tilescan wedge images, which were taken at 5× magnification, and neurite projection images, which were taken at 20× magnification.

Flow cytometry. Cells were dissociated into a single cell suspension with either TrypLE or Accutase, as noted above. Cells were pelleted via centrifugation and then resuspended into blocking buffer (5% FBS in DPBS). The samples were then spun down again and resuspended in 100 μL of blocking buffer per sample. For immunolabeling prior to flow cytometry, cells were incubated for 15 min in blocking buffer on ice. Cells were immunolabeled with an Alexa Fluor 647 conjugated mouse monoclonal antibody for c-myc tags (clone 9B11, Cell Signaling Technologies) at a 1:50 dilution for H9 activation experiments and with a Human Cadherin-6/KCAD Alexa Fluor 647-conjugated antibody (clone 427909, R&D Systems) for determination of K-cadherin expression. After staining, the samples were then washed twice with 200 μL blocking buffer, collected by centrifugation and then resuspended for analysis in 400 μL of blocking buffer. Flow cytometry results were collected from a Cellstream analytical flow cytometer and analyzed in FlowJo.

ELISA. For ELISA analysis, the Human TNF RI/TNFRSF1A DuoSet

ELISA kit and DuoSet Ancillary Reagents (R&D Systems) were used. Culture media were aspirated off the cells and media from conditions with GFP added were diluted 1:100 in reagent diluent while media from conditions without GFP added were diluted 1:10. Following the manufacturer's protocol, absorbance measurements at 450 nm were made on a Tecan Infinite M1000 Pro plate reader, with a measurement at 540 nm to correct for plate absorbance. Average absorbance of the 0 pg/mL standard was subtracted from all samples to correct for baseline absorbance. A standard curve was determined by plotting the log of the standard concentrations versus the log of absorbances. After fitting a linear best-fit line, the trendline equation was used to calculate the sample concentrations.

Quantitative real-time PCR. Cells were lysed and mRNA was isolated using the PureLink RNA Mini Kit (Invitrogen). mRNA was reverse transcribed into cDNA for qRT-PCR analysis using the SuperScript IV VILO Master Mix (Invitrogen). Samples were analyzed with the Power-Track SYBR Green Master Mix (Applied Biosystems) on a Bio-Rad CFX96 using a non-skirted low-profile plate (Thermo Scientific) with optical adhesive film (Applied Biosystems). The primers used are listed in Supplementary Table 1 [65,66]. Relative gene expression was calculated using the delta-delta Ct method using *r18s* as a reference gene and indicated samples as controls.

Immunocytochemistry. Cells were fixed in 2% paraformaldehyde in PBS for 10 min, washed in ice cold DPBS, and permeabilized and blocked in 0.3% Triton-X (EMD Millipore) and 5% FBS in PBS for 45 min. Cells were then stained for Tuj1 expression with an anti-Tuj1 mouse antibody conjugated to Alexa-Fluor 647 (product number 801210, Biolegend) diluted 1:500 in permeabilization and blocking buffer for 1 h at room temperature. The cells were then incubated in DPBS for 5 min and then counterstained with a 1:1000 dilution of DAPI (Thermo Scientific) in deionized water for 1 h.

Statistical analysis. All bar graphs display means of triplicates with error bars showing standard error of the mean. For experiments involving only two comparisons, statistical significance was determined with a Student's t-test or Welch's *t*-test, as appropriate based the distribution of variances, and with alpha set to 0.05. To determine significance in experiments involving >2 groups or categorical variables, one-way or two-way ANOVA was used as appropriate followed by Tukey's post-hoc test with alpha set at 0.05.

3. Results

3.1. Biomaterial surfaces co-opted to interface with synNotch cells

While synNotch is inspired by a juxtacrine cell-cell signaling receptor, our goal was to engineer biomaterial surfaces to capture soluble factors and thereby transduce artificial signaling via synNotch [40]. The synNotch platform is composed of two key elements (Fig. 1A): (1) the receptor protein that can be programmed to detect selected cues and (2) the "payload," or the genetic response element, which prescribes the outcome of induced synNotch signaling. The intracellular domain of the synNotch receptor used in these studies consists of the tetracycline-controlled transactivator (tTA), which activates expression of genes downstream of the TRE-inducible promoter. In this work, we establish the cell-substratum platform performance by enabling cells to respond to the bioinert protein GFP – a ligand that does not typically activate signaling in cells. To convert soluble GFP to an input detected by synNotch cells through interactions with biomaterials, we used a GFP-recognizing nanobody called LaG16 (K_d of 0.7 nM) to generate the recognition domain of the synNotch receptor protein [62]. In initial studies, the payload consists of bicistronic expression of firefly luciferase and mCherry reporter transgenes. Via lentiviral transduction, we engineered L929 fibroblasts to express the LaG16-synNotch receptor and inducible mCherry and luciferase payload. To enable biomaterials to capture soluble GFP for synNotch recognition, we functionalized cell culture surfaces with a GFP-specific nanobody, GFP-TRAP (K_d of 0.59

nM), conjugated to a polyethylene glycol (PEG) linker. The GFP-TRAP nanobody binds an epitope of GFP that does not overlap with the binding site of LaG16 [62].

To verify that this surface engineering strategy enables efficient synNotch activation, we compared activation via material-mediated immobilization of soluble GFP to the canonical synNotch activation mode of cell-cell juxtacrine signaling [40]. For juxtacrine signaling, GFP ligand expressing "sender" cells were engineered for transmembrane expression of GFP. Median mCherry fluorescence intensity values, as measured by flow cytometry, indicate that supplementation of medium with 5 nM GFP activates synNotch in a manner that depends on material surface programming with GFP-TRAP (Fig. 1B). Using this readout, material- and ligand-dependent activation levels exceeded 18-fold as compared to control conditions. Critically, addition of free GFP alone was inadequate to activate synNotch; biomaterial functionalization with the GFP-TRAP affinity motif was both necessary and sufficient to convert soluble GFP to a productive synNotch input. Further, synNotch activation via the ligand-capturing biomaterial compares favorably to juxtacrine activation of synNotch, which generated activation levels of 7-fold over control conditions. Greater activation via material-mediated capturing of soluble GFP may be due to increased density of ligand presented on functionalized culture surfaces as compared to membrane-bound ligand in engineered GFP-expressing cells. Based on these results, we determined that co-engineering synNotch cells and biomaterial surfaces represents a viable strategy to govern gene expression on the basis of soluble inputs in the cellular microenvironment.

Next, we assessed the sensitivity of the MATRIX signaling platform to varying concentrations of GFP input. We found that synNotch cells upregulate luciferase transgene expression at concentrations as low as 0.5 nM, exhibiting a roughly 100-fold increase in signal over background conditions (Fig. 1C). We found that the luminescence response begins to plateau at 2 nM GFP and reaches a maximal activation level at 5 nM GFP, illustrating induction of approximately 200-fold over basal conditions. Finally, to ascertain whether the platform could respond to levels of ligand secreted by cells, we engineered an L929 line to constitutively secrete GFP. We then co-cultured GFP secretors with synNotch cells on control or functionalized surfaces and observed ~36-fold luciferase upregulation in response to GFP ligand in a material-dependent manner (Fig. 1D). Thus, our strategy of integrating material surface engineering with cell design facilitates synthetic signaling that is tunable to ligand concentrations relevant to paracrine inputs and that display well over two orders of magnitude in dynamic range.

3.2. Flexible input selection

We then transitioned to test whether MATRIX could accommodate signaling inputs other than GFP. To achieve this, we exchanged the LaG16 extracellular motif for a nanobody known as LaM8, which recognizes red fluorescent protein (RFP) derivatives, including mCherry. We utilized magnetic beads functionalized with an anti-c-myc antibody as the ligand-capturing entity in this system, which made use of a c-myc-tagged mCherry. Upon input of c-myc-tagged mCherry, LaM8-synNotch L929 fibroblasts activate robustly and produce significant luciferase expression in a material- and ligand-dependent manner (Fig. 2A). Building off this, we then explored whether we could layer two artificial signaling circuits into a single cell population. We coupled the mCherry/LaM8 signal activation to the output of upstream activator sequence (UAS) promoter-driven Renilla luciferase expression, while GFP/LaG16 signal transduction produced firefly luciferase expression as in earlier experiments (Fig. 2B). We observed that transgene activation depended on provision of both the relevant ligand as well as cognate biomaterial (Fig. 2C). Of note, when cells were cultured in conditions that enabled simultaneous activation via both GFP and RFP inputs, the GFP-activated circuit reached just over 50% of its maximum activation level. We attribute this apparent partial activation of the firefly luciferase
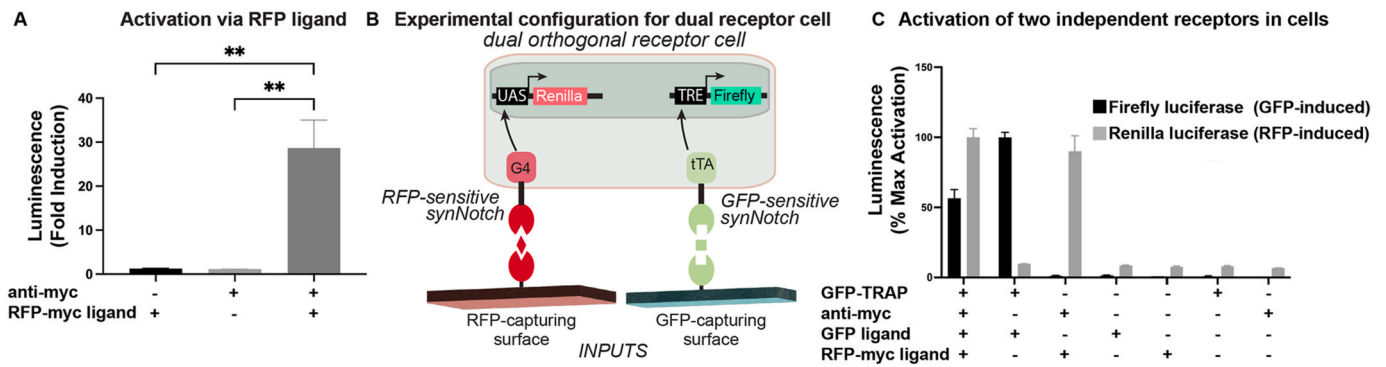
Fig. 2. The cell-biomaterial design strategy enables discrete programmable responses from multiple ligands. (A) Relative luminescence values indicating activity of the RFP-sensitive synNotch receptor to surface-captured mCherry-myc (one-way ANOVA with Tukey's post-hoc test; **p < 0.01). (B) Schematic of a dual receptor synNotch cell sensitive to RFP (output: Renilla luciferase) and GFP (output: firefly luciferase). (C) L929 mouse fibroblast cells programmed as in (B) were exposed to a variety of substrata and ligand conditions. Firefly and Renilla luminescence values were measured for each condition and plotted as a percent of the maximum activation value for each luminescence type. In all plots, n = 3 replicates; error bars indicate SEM.

transgene to interference of the anti-c-myc beads with the luminescence assay. Crucially, cross-activation of the two independent receptors was not observed. This indicates that multiple orthogonal receptors can be layered into a cell population, and activation can be achieved through selective material programming and ligand provision.

3.3. Spatially constrained artificial signaling

A key feature of synNotch is the requirement for mechanical strain to activate signaling [44]. As such, synNotch activation is highly localized. This opens the intriguing opportunity to capitalize on our cell-material

engineering strategy to develop a platform that produces user-specified, spatially restricted responses to bulk soluble cues. To test this, we used a cylindrical cell culture insert divided into four wedges (Ibidi) to constrain the pattern of functionalized cell culture surfaces. Cell culture surfaces were programmed with GFP-TRAP such that two out of four wedges could capture the soluble synNotch ligand GFP, while the remaining wedges were untreated and therefore unable to immobilize soluble GFP (Fig. 3A). This resulted in alternating wedges functionalized to capture GFP, which potentiates activation of the GFP-sensitive LaG16-synNotch via ligand immobilization within those wedges. After functionalization, the Ibidi insert was removed, and L929
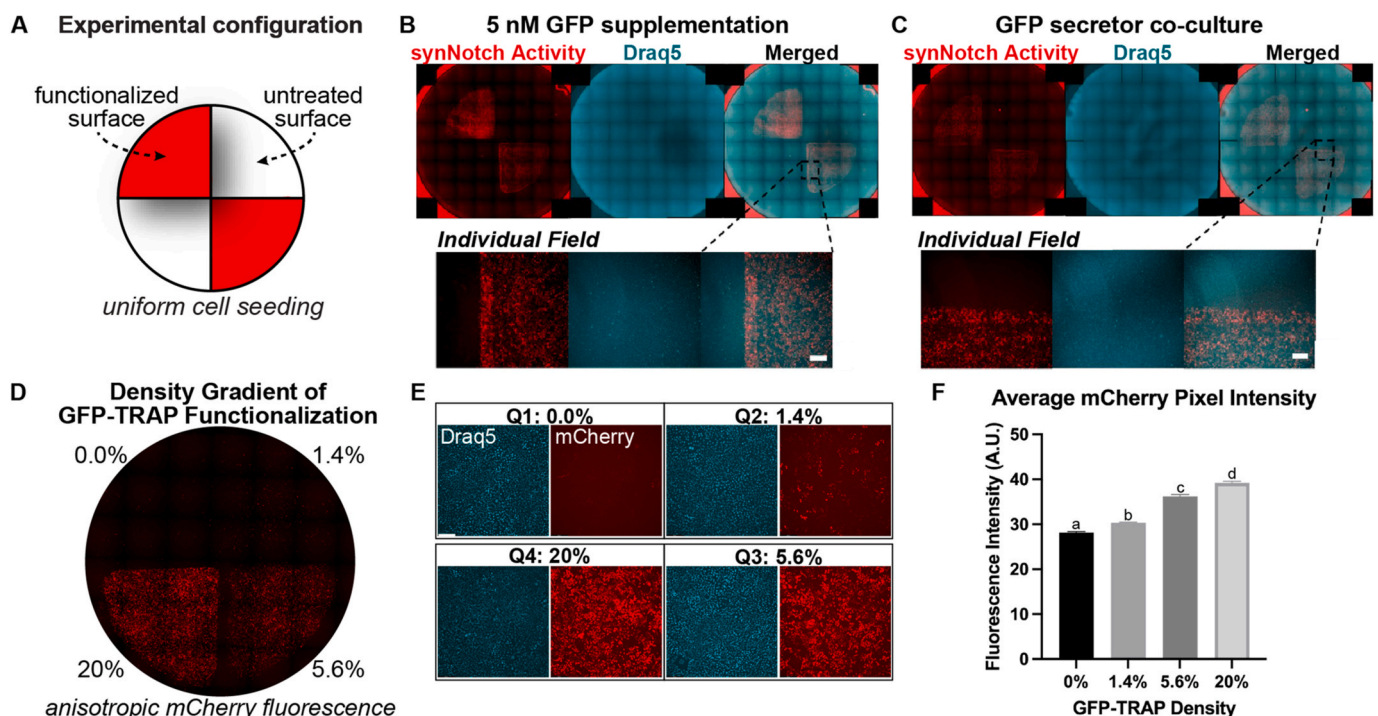

Fig. 3. Patterned surface functionalization results in spatially discrete mCherry expression in response to bulk GFP provision. (A) As illustrated, alternating wedges were functionalized with GFP-TRAP to organize synthetic signaling in response to the global cue of soluble GFP. The wedge chamber was removed prior to addition of GFP uniformly to the cell culture well. (B) synNotch activation, indicated by mCherry signal, induced by 5 nM GFP supplementation. Nuclear Draq5 counterstain was used to determine the distribution of cells across the cell culture well. (C) As in (B), except synNotch cells were mixed 1:1 with GFP-ligand secreting cells, indicating that the spatial gating is achievable at levels of ligand produced by cells. (D) Tilescan image of mCherry intensity after functionalization of wedge regions with GFP-TRAP preparations of 0%, 1.4%, 5.6%, or 20%. (E) Representative images of individual 10× objective fields from the tilescan shown in (D). (F) Quantified pixel intensities of 10× objective fields from wedges produced as shown in (D). n = 12 fields of view from replicate wedges. Groups not sharing same letters are significantly different (p < 0.0001, one-way ANOVA with Tukey's post-hoc). (Scale bar = 200 μm).

fibroblasts engineered with the LaG16-synNotch receptor driving mCherry transgene expression were plated throughout the whole well. The medium was supplemented with 5 nM GFP. After 48 h, the cells were stained with the nuclear dye Draq5 and imaged by microscopy. MCherry expression was constrained to wedge regions functionalized with GFP-TRAP (Fig. 3B). We repeated this experimental setup, replacing the 5 nM GFP with GFP-secreting L929 cells co-cultured with LaG16-synNotch cells at a 1:1 ratio. Consistent with prior results, synNotch cells were able to respond to GFP input in a pattern specified by surface functionalization (Fig. 3C). This illustrates that selective functionalization of biomaterial substrata enables spatial control over synNotch transgene expression, even in the presence of a uniform bath of activating factors, highlighting the utility of our approach of leveraging synNotch to organize cellular responses to bulk environmental cues.

We then queried whether we could obtain a graded response to bulk GFP inputs by varying the concentration of GFP-TRAP used to functionalize surfaces of each quadrant of the cell culture inserts. We used solutions of 0%, 1.4%, 5.6%, or 20% GFP-TRAP to functionalize culture surfaces defined by quadrants of the inserts. We then uniformly plated cells in the well and applied 5 nM GFP. Results demonstrate graded mCherry fluorescence intensity in accordance with increasing GFP-TRAP concentration, with a significant increase in mCherry pixel intensity at each level of GFP-TRAP applied to the surface (Fig. 3D–F). These data illustrate that MATRIX can be flexibly deployed to generate graded responses to soluble cues within a microenvironment.

Taken together, these studies establish the sensitivity, flexibility, and utility for spatially gating transgene expression with this co-developed cell-biomaterial platform.

3.4. MATRIX for CRISPR regulation

We then transitioned to illustrating diverse functions that the MATRIX platform can govern. Recent efforts in regenerative engineering have focused on deploying CRISPR epigenetic regulators *in vivo* [67]. To assess whether we could leverage MATRIX to control CRISPR-based transcriptome regulators, we engineered an L929 fibroblast cell line for inducible expression of the RNA-editing *Ruminococcus flavefaciens* XPD3002 Cas protein (CasRx) [63]. CasRx, in conjunction with gRNAs specific to a gene of interest, acts as a compact RNA-targeting CRISPR system and can mediate gene knockdown directly at the transcript level. To demonstrate proof-of-principle of MATRIX performance in this application, we engineered GFP-sensitive synNotch cells to activate CasRx expression in response to synNotch signaling. Cells were further engineered to constitutively express a single bicistronic transcript consisting of a K-cadherin cell adhesion molecule, IRES, and mCherry. Finally, we added a panel of four CasRx gRNAs specific to the mCherry transcript (Fig. 4A) [63]. As both K-cadherin and mCherry are expressed

through a single mRNA transcript, degradation of one portion of the transcript mediated by CasRx will knock down expression of both proteins. SynNotch cells were then plated onto the biomaterial to assess ligand-dependent CasRx knockdown efficiency after 72 h. Results illustrate that MATRIX rendered significant knockdown of both mCherry (Fig. 4B) and K-cadherin (Fig. 4C) in a GFP-dependent manner. These studies indicate that MATRIX may serve as a useful platform to orchestrate both cell delivery and transcriptome editing in transplanted cells.

3.5. MATRIX to attenuate inflammatory signaling

After highlighting features of the MATRIX platform in L929 fibroblasts, we aimed to extend this platform to other cell types. Due to their tri-lineage multipotency and an inherent ability to counteract dysregulated inflammation [68,69], marrow-derived mesenchymal stem cells (MSCs) represent a cell type of wide interest in regenerative engineering [70]. Thus, we first evaluated whether MSCs were operational in the context of MATRIX. We transduced mouse MSCs (mMSCs) with the GFP-sensitive LaG16 synNotch receptor linked to production of the transgene secreted alkaline phosphatase (SEAP). We then cultured the mMSCs with and without GFP and on control versus programmed biomaterial surfaces. We observed a significant increase in SEAP production as measured by a chemiluminescence assay (Fig. 5A), demonstrating that the design of MATRIX accommodates engineered MSCs.

We then extended these findings to determine whether MATRIX can augment the therapeutic potential of MSCs. TNF is frequently dysregulated in autoimmune and chronic inflammatory environments [71]. Thus, the ability to blunt TNF in tissues with tunable, local therapeutics represents a goal in regenerative medicine [72]. We replaced the SEAP transgene payload with the soluble TNF receptor type 1 (sTNFR1), which we and others have used as an antagonist of the pro-inflammatory cytokine TNF [66,73]. To demonstrate the ability of MATRIX to generate sTNFR1 production, we cultured synNotch mMSCs on control or functionalized surfaces and in the presence or absence of 5 nM GFP (Fig. 5B). As measured by ELISA, we observe a significant increase in sTNFR1 production, up to 49 ng/mL, when the cells are exposed to GFP on the ligand-capturing biomaterial, even with exposure to 10 ng/mL TNF (Fig. 5C).

We next analyzed whether this sTNFR1 production could antagonize deleterious levels of TNF. To monitor TNF signaling, we transduced mMSCs with a fluorescent mKate2 reporter [74] as a readout of NF-κB transcriptional activity. MSCs were then cultured on functionalized surfaces and in conditions of 0 versus 5 nM GFP with 0 versus 10 ng/mL TNF. As assessed by flow cytometry, we observed significant GFP-dependent reduction of mKate2 intensity, suggesting a decrease in TNF-induced NF-κB activity (Fig. 5D). We therefore performed gene
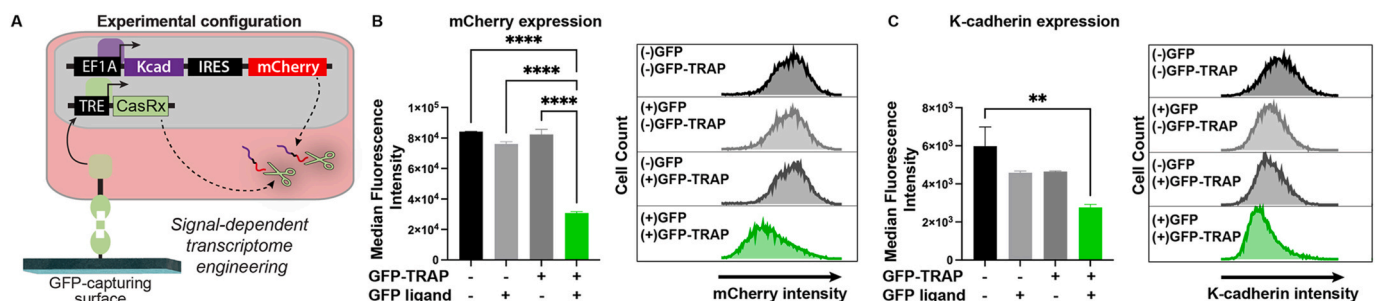

Fig. 4. The MATRIX platform facilitates CRISPR-based transcriptome modification. (A) Illustration of L929 cells used in this experiment. Cells were engineered to constitutively express a single transcript encoding K-cadherin and mCherry. SynNotch activation leads to expression of CasRx. Vectors enabling expression of the mCherry-targeting gRNAs, which enable CasRx to initiate degradation of mCherry-encoding transcripts, are not shown. (B) Left: Median fluorescence intensity of mCherry in cells exposed to 0 nM or 50 nM GFP, as assessed by flow cytometry. Right: Representative histograms of mCherry expression of cells with and without the GFP-capturing surface in 0 or 50 nM GFP conditions. (C) Left: Median fluorescence intensity of anti-K-cadherin staining in cells with and without the GFP-capturing surface and exposed to 0 nM or 50 nM GFP, as assessed by flow cytometry. Right: Representative histograms of anti-K-cadherin staining of cells in 0 or 50 nM GFP conditions. In all plots, **p < 0.01 and ****p < 0.0001, two-way ANOVA with Tukey's post-hoc test. n = 3 replicates; error bars indicate SEM.
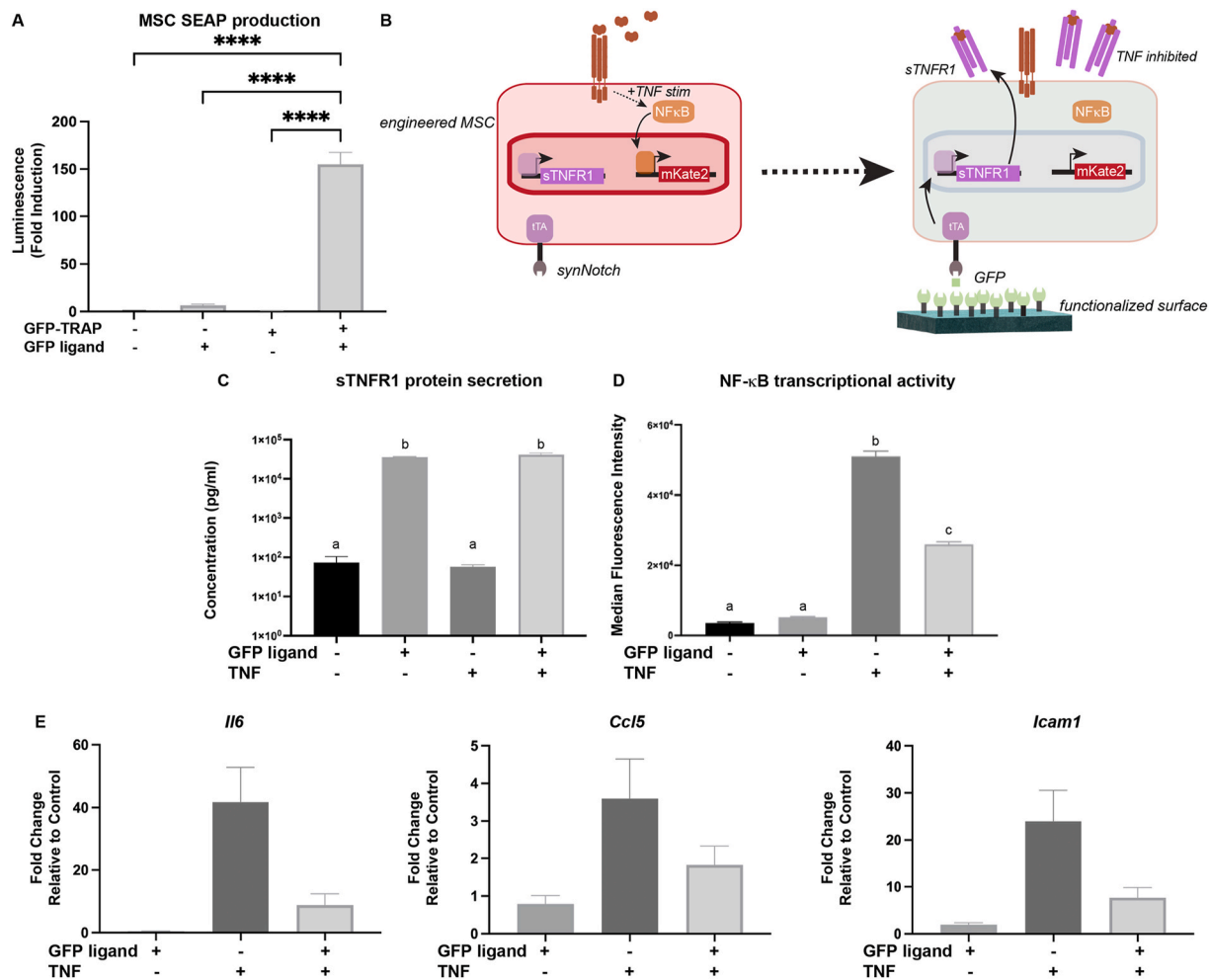
Fig. 5. Therapeutic behaviors of mesenchymal stem cells can be governed via the MATRIX design approach. (A) SEAP reporter transgene expression from murine MSCs in a surface- and synNotch-ligand dependent manner. (****p < 0.0001 b y two-way ANOVA with Tukey's post-hoc test). (B) Schematic of experimental configuration in panels C–E. (C) synNotch-dependent sTNFR1 expression in response to GFP input and TNF treatment. Groups not sharing the same letters are statistically significantly different by two-way ANOVA with Tukey's post-hoc test. (D) Median fluorescence intensity of an mKate2 reporter expressed from tandem repeats of NF-κB response elements. Groups not sharing the same letters are statistically significantly different by two-way ANOVA with Tukey's post-hoc test. (E) qRT-PCR gene expression profiling of transcripts upregulated by TNF treatment of MSCs.

expression analysis to determine whether a panel of genes regulated by TNF in MSCs reflected a GFP-dependent profile. We observed reduced expression of the inflammatory markers *Il6*, *Ccl5*, and *Icam1* (Fig. 5E). Collectively, these results indicate that MSCs integrated into the MA-TRIX platform can effectively antagonize pro-inflammatory cytokine signaling.

3.6. MATRIX to orchestrate pluripotent stem cell differentiation

A crucial aspect of regenerative engineering relies on the ability to produce target cell types and neotissue from stem cells. As such, we investigated whether the MATRIX platform could regulate transgene expression in human pluripotent stem cells (hPSCs). Such a goal represents a non-trivial extension of the MATRIX platform, since hPSCs require basement membrane proteins, such as Matrigel, as substrata to support cell attachment and viability during subcultivation and differentiation. To develop a cell culture surface capable of capturing syn-Notch ligand and compatible with hPSC maintenance and differentiation, we turned to a fully defined, peptide-based substratum comprised of a glycosaminoglycan binding-peptide (GBP) [53] and cyclic arginine-glycine-aspartate (cRGD) for cell adhesion [54], with GFP-TRAP incorporated to facilitate immobilization of soluble GFP. We engineered H9 human embryonic stem cells (hESCs) to express a

GFP-sensitive synNotch receptor with a downstream gene circuit that induces mCherry upon synNotch activation. Flow cytometry indicates potent activation of synNotch signaling in engineered H9 hESCs (Fig. 6A). These results illustrate that the MATRIX design platform ac-commodates synthetic, orthogonal signaling in hPSCs.

We then extended these findings to determine whether the MATRIX platform can mediate synthetic signaling that drives hPSC differentiation. We engineered H9 hESCs to express mCherry and neurogenin-2 (Ngn2), a master transcription factor capable of converting hPSCs to TUJ1+ motor neurons upon ectopic expression [64,75,76]. We then cultured these cells on the defined GBP/cRGD/GFP-TRAP surface previously used. As expected, GFP ligand robustly activated synNotch in H9 hESCs (Fig. 6B). We also found that, after 4 days, GFP-induced Ngn2 expression gave rise to a TUJ1+ population of cells displaying extensive neurite projections, whereas the 0 nM GFP group did not adopt this fate (Fig. 6C). These results show that integration of the MATRIX platform with purpose-driven cell design enables coordination of pluripotent stem cell differentiation.

4. Discussion

Here, we present the concept of co-developing engineered cells and designer biomaterial surfaces to generate a privileged channel of
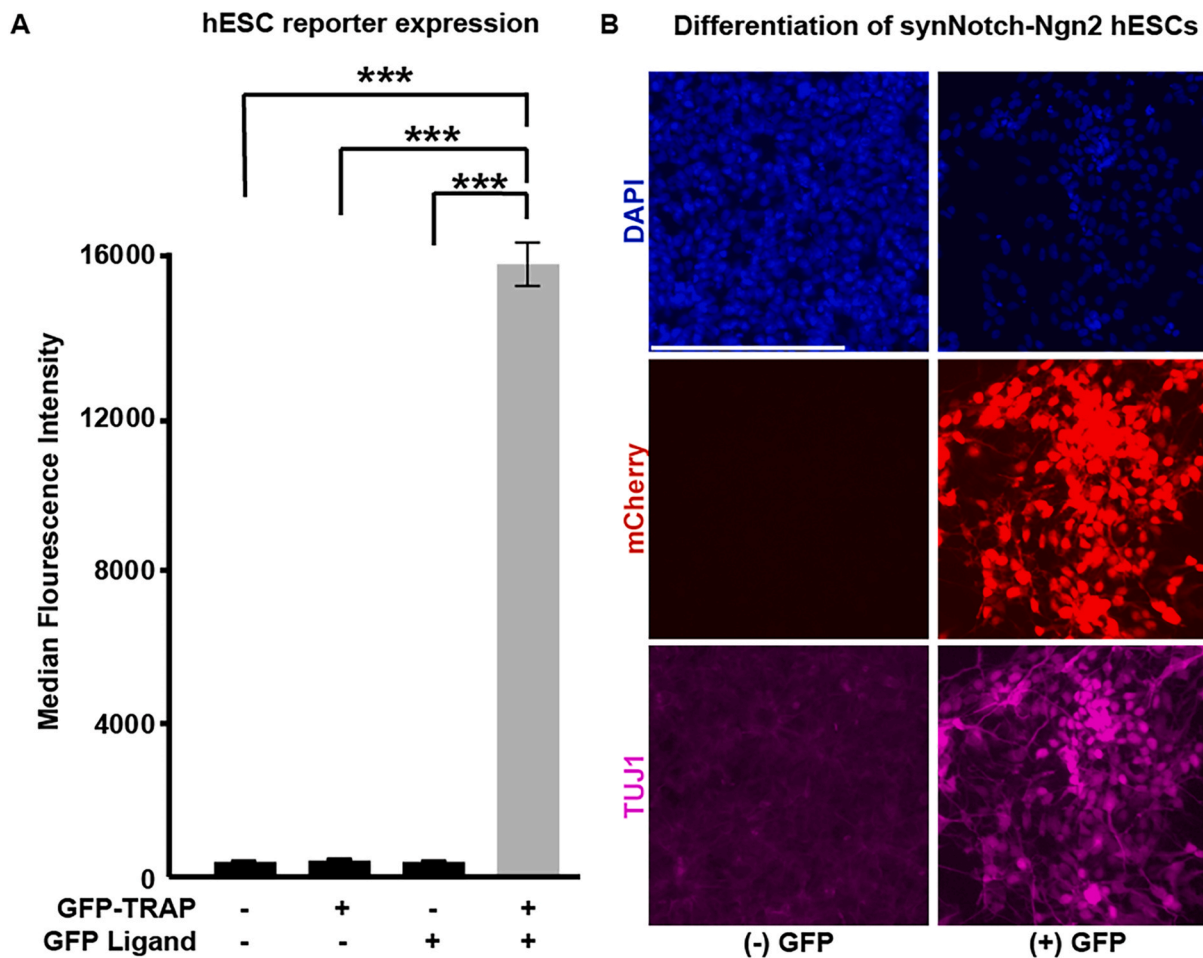
A
hESC reporter expression

B
Differentiation of synNotch-Ngn2 hESCs

Fig. 6. The MATRIX design approach enables artificial cell-substratum signaling in human pluripotent stem cells. (A) Median fluorescence intensity of the reporter transgene mCherry in synNotch H9 hESCs. (***$p < 0.001$; n = 3 replicates; two-way ANOVA with Tukey's post-hoc test). (B) Fluorescence microscopy of H9 cells engineered to inducibly express the master regulator of neurogenesis, Ngn2. Top: DAPI nuclear stain; Middle: mCherry fluorescence reporter co-expressed with Ngn2; Bottom: anti-TUJ1 immunocytochemistry. Scale bar = 200 μm.

communication via artificial signaling networks. Our platform, referred to as MATRIX, combines synthetic biology and biomaterial design to customize cell functions for regenerative engineering applications. The MATRIX platform is highly flexible, in that both cells and material surfaces can be programmed to interact via arbitrarily selected ligands. Here, we demonstrate that two different bioinert ligands, GFP and mCherry, can be converted to productive signaling factors. We show that the MATRIX platform can support orthogonal receptors that sense distinct inputs, implement discrete cellular functions, and do not crosstalk. Our data indicate that cell responses to such inputs can be customized for defined applications relevant to regenerative medicine, including orchestration of spatial responses to bulk soluble inputs, regulation of CRISPR-based transcriptome modifiers, resolution of inflammatory signaling, and hPSC differentiation.

The bulk of these experiments used the bioinert protein GFP as the synNotch signaling factor. With soluble GFP as a ligand, we produced a MATRIX configuration with a dynamic range exceeding 200-fold, with robust activation by GFP concentrations as low as 0.5 nM as well as cell secreted GFP. For the majority of these studies, we chose high affinity motifs for programming the biomaterial surface (GFP-TRAP, $K_d = 0.59$ nM [62]) and the synNotch receptor (LaG16, $K_d = 0.7$ nM [62]). Though not explored here, selection of a different affinity motif for either biomaterial functionalization or for synNotch receptor design would facilitate tunable sensitivity. In fact, in a subset of this work, we made use of a lower affinity LaG17-based synNotch receptor ($K_d = 50$ nM [62]), illustrating flexibility in the overall configuration of MATRIX.

In principle, the MATRIX framework for co-engineering cells and biomaterial surfaces can accommodate any ligand. The major design constraint of MATRIX is the availability of two affinity motifs that can simultaneously bind target ligand: one that allows ligand recognition by the synNotch receptor and the other to enable surface immobilization of the soluble input. We anticipate future studies will entail selection of non-native factors other than GFP or mCherry for orthogonal control of cell behaviors. Further, because the system can also be adapted to re-route native inputs, such as morphogens or pro-inflammatory cytokines, we believe the MATRIX platform opens the intriguing possibility to customize cell delivery vehicles to respond to typically deleterious factors in a microenvironment and produce therapeutic factors on demand.

Several sophisticated biomaterial platforms have been reported as dynamic vehicles for influencing cell behaviors. Examples include materials that present immunomodulatory/anti-inflammatory factors [77–81], differentiation factors [82–85], chemokines [86], and angiogenic factors [87,88]. Presented in the form of hydrogels [89–92], polymeric scaffolds [93–98], and nanoparticles [99–102], these materials can adapt to environmental cues such as light [103–105], pH [106], enzyme-mediated degradation [107], and temperature [108,109]. Such designs support the controlled release of therapeutic factors, bypassing the need for bolus delivery. However, once the structures housing these bioactive factors degrade as designed to promote release, these biomaterial matrices can no longer provide selected cues to cells in the environment. Engineered living materials (ELMs) have also been created by

combining microorganisms, such as bacteria and yeast, with bio-materials [110]. These platforms hold promise for use as self-growing, anti-fungal adhesive wound patches or for the sustained release of drugs such as antibiotics; however, they are limited to the extent that microorganisms can be applied as agents of tissue regeneration and repair. Further, advances in niche-responsive gene regulation are required to reliably control activities of transplanted microorganisms in ELMs [111]. To circumvent these potential shortcomings, our MATRIX platform weds synthetic biology with biomaterial design to generate a tunable, inducible platform capable of sustaining localized transgene production of therapeutic factors via orthogonal signaling of engineered mammalian cells. By designing a platform that integrates material-mediated signal transduction with engineered cells, our plat-form organizes cell behaviors, instructs differentiation programs, and enables cells to serve as inducible biologic drug delivery agents to sculpt a regenerative niche. Thus, the MATRIX platform complements advances in biomaterial design to offer a modular, flexible platform for regenerative engineering. Continued development of MATRIX will pursue extension of the platform from 2D surfaces to 3D hydrogels and scaffolds.

Numerous synthetic receptor platforms have been adapted to exert exquisite control over cell functions. Many of these are designed to detect soluble cues including bioactive ligands like VEGF or rapamycin, as well as pharmacologically inert factors like GFP, azo dyes, or cloza-pine-*N*-oxide [45–48,112–115]. While these platforms are extraordinarily useful, signal transduction via such receptors is sensitive to ligand concentration rather than ligand immobilization. The MATRIX platform constrains ligand-induced responses to regions occupied by pro-grammed biomaterial surfaces, taking advantage of a main feature of Notch signaling, requiring co-localization of the soluble ligand, the biomaterial, and the engineered cell for a response while also being responsive to ligand concentration with tunable activation [116]. Thus, in conditions in which local tissue targeting or spatial regulation of cell functions are central, such as restricted production of pleiotropic factors or templating of heterogenous neotissue constructs, the MATRIX framework offers an avenue for gating responses of engineered cells to bulk soluble inputs.

In conclusion, we present MATRIX as a solution to the challenge of designing custom cell-matrix interactions to control therapeutic activities of cells. This platform combines advances in the areas of cell design and biomaterial engineering. Artificial signaling enabled by MATRIX spatially coordinates engineered cellular responses to bulk soluble factors. Our use of MATRIX facilitated CRISPR-based knockdown of specific gene targets, demonstrating the ability to leverage cell carriers and tis-sue engineering scaffolds as vehicles to modulate transcriptional pro-grams of engineered cells upon transplantation. We also used MATRIX to augment the inflammation attenuation of mesenchymal stem cells, a behavior relevant to development of cell-based therapies to treat auto-immune diseases [117,118], arthropathies [119], and neuro-degeneration [120,121]. Finally, we illustrate that the MATRIX framework allows for inducible, material-mediated differentiation of hPSCs, indicating applicability of this platform for production of cell or tissue replacements. We have thus demonstrated that MATRIX makes it possible to finely regulate cellular responses to selected inputs with engineered specificity and targeted outputs that are tunable in magni-tude, making it a platform suitable for filling several needs in regener-ative engineering.

Competing interests

W.A.L holds equity in Gilead and Intellia and is an adviser for Allo-gene Therapeutics. W.A.L and J.M.B have filed patent disclosures related to this work.

Credit author statement

Joanne C. Lee: Conceptualization, Validation, Formal analysis, Investigation, Writing – Original Draft, Writing – Review & Editing, Visualization. Hannah J. Brien: Conceptualization, Validation, Formal analysis, Investigation, Writing – Original Draft, Writing – Review & Editing, Visualization. Bonnie L. Walton: Validation, Formal analysis, Investigation, Writing – Original Draft, Writing – Review & Editing, Visualization. Zachary M. Eidman: Validation, Formal analysis, Inves-tigation, Writing – Review & Editing Satoshi Toda: Resources, Writing – Review & Editing. Wendell A. Lim: Conceptualization, Writing – Review & Editing, Project administration, Funding acquisition. Jonathan M. Brunger: Conceptualization, Validation, Formal analysis, Investigation, Writing – Original Draft, Writing – Review & Editing, Visualization, Project administration, Funding acquisition, Supervision.

Declaration of competing interest

The authors declare the following financial interests/personal re-lationships which may be considered as potential competing interests: Wendell A. Lim reports financial support was provided by National In-stitutes of Health. Wendell A. Lim reports financial support was pro-vided by Defense Advanced Research Projects Agency. Wendell A. Lim reports financial support was provided by Howard Hughes Medical Institute. Wendell A. Lim reports financial support was provided by National Science Foundation. Jonathan M. Brunger reports financial support was provided by Arthritis National Research Foundation. Jonathan M. Brunger reports financial support was provided by National Science Foundation. Jonathan M. Brunger reports financial support was provided by National Institutes of Health. Joanne C. Lee reports finan-cial support was provided by National Science Foundation. Hannah J. Brien reports financial support was provided by National Science Foundation. Bonnie L. Walton reports financial support was provided by National Science Foundation. Wendell A. Lim reports a relationship with Gilead Sciences Inc that includes: equity or stocks. Wendell A. Lim re-ports a relationship with Intellia Therapeutics Inc that includes: equity or stocks. Wendell A. Lim reports a relationship with Allogene Thera-peutics that includes: consulting or advisory. Wendell A. Lim has patent pending to University of California, San Francisco. Jonathan M. Brunger has patent pending to University of California, San Francisco.

Data availability

Data will be made available on request.

Appendix A. Supplementary data

Supplementary data to this article can be found online at https://doi.org/10.1016/j.biomaterials.2023.122099.

References

[1] U. Jammalamadaka, K. Tappa, Recent advances in biomaterials for 3D printing and tissue engineering, J. Funct. Biomater. 9 (2018) 22, https://doi.org/10.3390/jfb9010022.

[2] F.J. O'Brien, Biomaterials & scaffolds for tissue engineering, Mater. Today 14 (2011) 88–95, https://doi.org/10.1016/S1369-7021(11)70058-X.

[3] R. Rhanna, A. Hasan, Introduction to tissue engineering, in: Tissue Engineering for Artificial Organs, Wiley-VCH Verlag GmbH & Co. KGaA, Weinheim, Germany, 2017, pp. 1–34, https://doi.org/10.1002/9783527689934.ch1.

[4] S.M. Naqvi, L.M. McNamara, Stem cell mechanobiology and the role of biomaterials in governing mechanotransduction and matrix production for tissue regeneration, Front. Bioeng. Biotechnol. 8 (2020) 1375, https://www.frontiersin.org/articles/10.3389/fbioe.2020.597661/full.

[5] T.E. Brown, K.S. Anseth, Spatiotemporal hydrogel biomaterials for regenerative medicine, Chem. Soc. Rev. 46 (2017) 6532, https://doi.org/10.1039/C7CS00445A.

[6] K. Uto, J.H. Tsui, C.A. DeForest, D.H. Kim, Dynamically tunable cell culture platforms for tissue engineering and mechanobiology, Prog. Polym. Sci. 65 (2017) 53–82, https://doi.org/10.1016/J.PROGPOLYMSCI.2016.09.004.

[7] P. Bajaj, R.M. Schweller, A. Khademhosseini, J.L. West, R. Bashir, 3D biofabrication strategies for tissue engineering and regenerative medicine, Annu. Rev. Biomed. Eng. 16 (2014) 247–276, https://doi.org/10.1146/annurev-bioeng-071813-105155.

[8] N.R. Labriola, J.S. Sadick, J.R. Morgan, E. Mathiowitz, E.M. Darling, Cell mimicking microparticles influence the organization, growth, and mechanophenotype of stem cell spheroids, Ann. Biomed. Eng. 46 (2018) 1146–1159, https://doi.org/10.1007/S10439-018-2028-4.

[9] C.L. Gilchrist, E.M. Darling, J. Chen, L.A. Setton, Extracellular matrix ligand and stiffness modulate immature nucleus pulposus cell-cell interactions, PLoS One 6 (2011), e27170, https://doi.org/10.1371/JOURNAL.PONE.0027170.

[10] W.J. Hadden, J.L. Young, A.W. Holle, M.L. McFetridge, D.Y. Kim, P. Wijesinghe, H. Taylor-Weiner, J.H. Wen, A.R. Lee, K. Bieback, B.N. Vo, D.D. Sampson, B. F. Kennedy, J.P. Spatz, A.J. Engler, Y.S. Cho, Stem cell migration and mechanotransduction on linear stiffness gradient hydrogels, Proc. Natl. Acad. Sci. U. S. A. 114 (2017) 5647–5652, https://doi.org/10.1073/PNAS.1618239114.

[11] J. Swift, I.L. Ivanovska, A. Buxboim, T. Harada, P.C.D.P. Dingal, J. Pinter, J. D. Pajerowski, K.R. Spinler, J.W. Shin, M. Tewari, F. Rehfeldt, D.W. Speicher, D. E. Discher, Nuclear lamin-A scales with tissue stiffness and enhances matrix-directed differentiation, Science (2013) 341, https://doi.org/10.1126/SCIENCE.1240104, 1979.

[12] N. Gjorevski, N. Sachs, A. Manfrin, S. Giger, M.E. Bragina, P. Ordóñez-Morán, H. Clevers, M.P. Lutolf, Designer matrices for intestinal stem cell and organoid culture, Nature 539 (2016) 560–564, https://doi.org/10.1038/nature20168.

[13] F.M. Watt, W.T.S. Huck, Role of the extracellular matrix in regulating stem cell fate, Nat. Rev. Mol. Cell Biol. 14 (2013) 467–473, https://doi.org/10.1038/nrm3620.

[14] W.L. Murphy, T.C. McDevitt, A.J. Engler, Materials as stem cell regulators, Nat. Mater. 13 (2014) 547–557, https://doi.org/10.1038/nmat3937.

[15] X. Liu, Y. Wang, Y. He, X. Wang, R. Zhang, A. Bachhuka, R. Madathiparambil Visalakshan, Q. Feng, K. Vasilev, Synergistic effect of surface chemistry and surface topography gradient on osteogenic/adipogenic differentiation of hMSCs, ACS Appl. Mater. Interfaces 13 (2021) 30306–30316, https://doi.org/10.1021/acsami.1c03915.

[16] Y. Zhu, H. Liang, X. Liu, J. Wu, C. Yang, T. Man Wong, K.Y. H Kwan, K.M. C Cheung, S. Wu, K.W. K Yeung, Regulation of macrophage polarization through surface topography design to facilitate implant-to-bone osteointegration, Sci. Adv. 7 (2021), https://doi.org/10.1126/sciadv.abf6654.

[17] S. Lee, A.E. Stanton, X. Tong, F. Yang, Hydrogels with enhanced protein conjugation efficiency reveal stiffness-induced YAP localization in stem cells depends on biochemical cues, Biomaterials 202 (2019) 26–34, https://doi.org/10.1016/j.biomaterials.2019.02.021.

[18] D. Zhu, P. Trinh, E. Liu, F. Yang, Biochemical and mechanical gradients synergize to enhance cartilage zonal organization in 3D, ACS Biomater. Sci. Eng. 4 (2018) 3561–3569, https://doi.org/10.1021/ACSBIOMATERIALS.8B00775.

[19] A. Khademhosseini, R. Langer, J. Borenstein, J.P. Vacanti, Microscale technologies for tissue engineering and biology, Proc. Natl. Acad. Sci. USA 103 (2006) 2480–2487, https://doi.org/10.1073/PNAS.0507681102.

[20] C.R. Rowland, D.P. Lennon, A.I. Caplan, F. Guilak, The effects of crosslinking of scaffolds engineered from cartilage ECM on the chondrogenic differentiation of MSCs, Biomaterials 34 (2013) 5802–5812, https://doi.org/10.1016/J.BIOMATERIALS.2013.04.027.

[21] C.M. Murphy, M.G. Haugh, F.J. O'Brien, The effect of mean pore size on cell attachment, proliferation and migration in collagen–glycosaminoglycan scaffolds for bone tissue engineering, Biomaterials 31 (2010) 461–466, https://doi.org/10.1016/J.BIOMATERIALS.2009.09.063.

[22] J.S. Miller, K.R. Stevens, M.T. Yang, B.M. Baker, D.H.T. Nguyen, D.M. Cohen, E. Toro, A.A. Chen, P.A. Galie, X. Yu, R. Chaturvedi, S.N. Bhatia, C.S. Chen, Rapid casting of patterned vascular networks for perfusable engineered three-dimensional tissues, Nat. Mater. 11 (2012) 768–774, https://doi.org/10.1038/nmat3357.

[23] D.B. Kolesky, R.L. Truby, A. Sydney Gladman, T.A. Busbee, K.A. Homan, J. A. Lewis, D.B. Kolesky, R.L. Truby, A.S. Gladman, T. Busbee, K.A. Homan, J. A. Lewis, 3D bioprinting of vascularized, heterogeneous cell-laden tissue constructs, Adv. Mater. 26 (2014) 3124–3130, https://doi.org/10.1002/ADMA.201305506.

[24] N.D. Evans, C. Minelli, E. Gentleman, V. LaPointe, S.N. Patankar, M. Kallivretaki, X. Chen, C.J. Roberts, M.M. Stevens, Substrate stiffness affects early differentiation events in embryonic stem cells, Eur. Cell. Mater. 18 (2009) 1–13, https://doi.org/10.22203/ECM.V018A01.

[25] S. Khetan, M. Guvendiren, W.R. Legant, D.M. Cohen, C.S. Chen, J.A. Burdick, Degradation-mediated cellular traction directs stem cell fate in covalently crosslinked three-dimensional hydrogels, Nat. Mater. 12 (2013) 458–465, https://doi.org/10.1038/nmat3586.

[26] A.J. Engler, S. Sen, H.L. Sweeney, D.E. Discher, Matrix elasticity directs stem cell lineage specification, Cell 126 (2006) 677–689, https://doi.org/10.1016/j.cell.2006.06.044.

[27] B. Trappmann, J.E. Gautrot, J.T. Connelly, D.G.T. Strange, Y. Li, M.L. Oyen, M. A. Cohen Stuart, H. Boehm, B. Li, V. Vogel, J.P. Spatz, F.M. Watt, W.T.S. Huck, Extracellular-matrix tethering regulates stem-cell fate, Nat. Mater. 11 (2012) 642–649, https://doi.org/10.1038/nmat3339.

[28] J.A. Hammer, J.L. West, Dynamic ligand presentation in biomaterials, Bioconjugate Chem. 29 (2018) 2140–2149, https://doi.org/10.1021/acs.bioconjchem.8b00288.

[29] F. Qu, J.L. Holloway, J.L. Esterhai, J.A. Burdick, R.L. Mauck, Programmed biomolecule delivery to enable and direct cell migration for connective tissue repair, Nat. Commun. 8 (2017) 1, https://doi.org/10.1038/s41467-017-01955-w, 1–11.

[30] C.C. Lin, P.D. Boyer, A.A. Aimetti, K.S. Anseth, Regulating MCP-1 diffusion in affinity hydrogels for enhancing immuno-isolation, J. Contr. Release 142 (2010) 384–391, https://doi.org/10.1016/J.JCONREL.2009.11.022.

[31] Y. Zhang, R. Wang, Y. Hua, R. Baumgartner, J. Cheng, Trigger-responsive poly (β-amino ester) hydrogels, ACS Macro Lett. 3 (2014) 693–697, https://doi.org/10.1021/mz500277j.

[32] R.J. Mumper, A.S. Huffman, P.A. Puolakkainen, L.S. Bouchard, W.R. Gombotz, Calcium-alginate beads for the oral delivery of transforming growth factor-β1 (TGF-β1): stabilization of TGF-β1 by the addition of polyacrylic acid within acid-treated beads, J. Contr. Release 30 (1994) 241–251, https://doi.org/10.1016/0168-3659(94)90030-2.

[33] A. Ovsianikov, S. Mühleder, J. Torgersen, Z. Li, X.-H. Qin, S. van Vlierberghe, P. Dubruel, W. Holnthoner, H. Redl, R. Liska, J. Stampfl, Laser photofabrication of cell-containing hydrogel constructs, Langmuir 30 (2014) 3787–3794, https://doi.org/10.1021/la402346z.

[34] D.Y. Kim, D.Y. Kwon, J.S. Kwon, J.H. Park, S.H. Park, H.J. Oh, J.H. Kim, B. H. Min, K. Park, M.S. Kim, Synergistic anti-tumor activity through combinational intratumoral injection of an in-situ injectable drug depot, Biomaterials 85 (2016) 232–245, https://doi.org/10.1016/J.BIOMATERIALS.2016.02.001.

[35] T. Shirakura, T.J. Kelson, A. Ray, A.E. Malyarenko, R. Kopelman, Hydrogel nanoparticles with thermally controlled drug release, ACS Macro Lett. 3 (2014) 602–606, https://doi.org/10.1021/MZ500231E.

[36] A.M. Kloxin, K.J.R. Lewis, C.A. Deforest, G. Seedorf, M.W. Tibbitt, V. Balasubramaniam, K.S. Anseth, Responsive culture platform to examine the influence of microenvironmental geometry on cell function in 3D, Integr. Biol. 4 (2012) 1540–1549, https://doi.org/10.1039/C2IB20212C.

[37] C.A. DeForest, K.S. Anseth, Photoreversible patterning of biomolecules within click-based hydrogels, Angew. Chem. Int. Ed. 51 (2012) 1816–1819, https://doi.org/10.1002/anie.201106463.

[38] B.P. Purcell, D. Lobb, M.B. Charati, S.M. Dorsey, R.J. Wade, K.N. Zellars, H. Doviak, S. Pettaway, C.B. Logdon, J.A. Shuman, P.D. Freels, J.H. Gorman, R. C. Gorman, F.G. Spinale, J.A. Burdick, Injectable and bioresponsive hydrogels for on-demand matrix metalloproteinase inhibition, Nat. Mater. 13 (2014) 653–661, https://doi.org/10.1038/nmat3922, 2014 13:6.

[39] J. Li, D.J. Mooney, Designing hydrogels for controlled drug delivery, Nat. Rev. Mater. 1 (2016), 16071, https://doi.org/10.1038/natrevmats.2016.71.

[40] L. Morsut, K.T. Roybal, X. Xiong, R.M. Gordley, S.M. Coyle, M. Thomson, W. A. Lim, Engineering customized cell sensing and response behaviors using synthetic Notch receptors, Cell 164 (2016) 780–791, https://doi.org/10.1016/J.CELL.2016.01.012.

[41] K.T. Roybal, J.Z. Williams, L. Morsut, L.J. Rupp, I. Kolinko, J.H. Choe, W. J. Walker, K.A. McNally, W.A. Lim, Engineering T cells with customized therapeutic response programs using synthetic Notch receptors, Cell 167 (2016) 419–432.e16, https://doi.org/10.1016/J.CELL.2016.09.011.

[42] K.T. Roybal, L.J. Rupp, L. Morsut, W.J. Walker, K.A. McNally, J.S. Park, W.A. Lim, Precision tumor recognition by T cells with combinatorial antigen-sensing circuits, Cell 164 (2016) 770–779, https://doi.org/10.1016/J.CELL.2016.01.011.

[43] S. Toda, L.R. Blauch, S.K.Y. Tang, L. Morsut, W.A. Lim, Programming self-organizing multicellular structures with synthetic cell-cell signaling, Science (2018) 156–162, https://doi.org/10.1126/science.aat0271.

[44] W.R. Gordon, B. Zimmerman, L. He, L.J. Miles, J. Huang, K. Tiyanont, D. G. McArthur, J.C. Aster, N. Perrimon, J.J. Loparo, S.C. Blacklow, Mechanical allostery: evidence for a force requirement in the proteolytic activation of Notch, Dev. Cell 33 (2015) 729–736, https://doi.org/10.1016/J.DEVCEL.2015.05.004.

[45] K. Krawczyk, L. Scheller, H. Kim, M. Fussenegger, Rewiring of endogenous signaling pathways to genomic targets for therapeutic cell reprogramming, Nat. Commun. 11 (2020), https://doi.org/10.1038/s41467-020-14397-8, 1–9.

[46] N.M. Daringer, R.M. Dudek, K.A. Schwarz, J.N. Leonard, Modular Extracellular sensor architecture for engineering mammalian cell-based devices, ACS Synth. Biol. 3 (2014) 892–902, https://doi.org/10.1021/SB400128G.

[47] H.I. Edelstein, P.S. Donahue, J.J. Muldoon, A.K. Kang, T.B. Dolberg, L. M. Battaglia, E.R. Allchin, M. Hong, J.N. Leonard, Elucidation and refinement of synthetic receptor mechanisms, Synth Biol 5 (2020) 17, https://doi.org/10.1093/SYNBIO/YSAA017.

[48] L. Scheller, T. Strittmatter, D. Fuchs, D. Bojar, M. Fussenegger, Generalized extracellular molecule sensor platform for programming cellular behavior, Nat. Chem. Biol. 14 (2018) 723–729, https://doi.org/10.1038/s41589-018-0046-z.

[49] G. Barnea, W. Strapps, G. Herrada, Y. Berman, J. Ong, B. Kloss, R. Axel, K.J. Lee, The genetic design of signaling cascades to record receptor activation, Proc. Natl. Acad. Sci. U. S. A. 105 (2008) 64–69, https://doi.org/10.1073/PNAS.0710487105.

[50] W.K. Kroeze, M.F. Sassano, X.P. Huang, K. Lansu, J.D. McCorvy, P.M. Giguère, N. Sciaky, B.L. Roth, PRESTO-Tango as an open-source resource for interrogation of the druggable human GPCRome, Nat. Struct. Mol. Biol. 22 (2015) 362–369, https://doi.org/10.1038/nsmb.3014, 2015 22:5.

[51] X. Huang, J.Z. Williams, R. Chang, Z. Li, C.E. Burnett, R. Hernandez-Lopez, I. Setiady, E. Gai, D.M. Patterson, W. Yu, K.T. Roybal, W.A. Lim, T.A. Desai, DNA scaffolds enable efficient and tunable functionalization of biomaterials for immune cell modulation, Nat. Nanotechnol. 16 (2021) 214–223, https://doi.org/10.1038/s41565-020-00813-z.

[52] S. Toda, W.L. McKeithan, T.J. Hakkinen, P. Lopez, O.D. Klein, W.A. Lim, Engineering synthetic morphogen systems that can program multicellular patterning, Science 370 (2020) 327–331, https://doi.org/10.1126/science.abc0033, 1979.

[53] J.R. Klim, L. Li, P.J. Wrighton, M.S. Piekarczyk, L.L. Kiessling, A defined glycosaminoglycan-binding substratum for human pluripotent stem cells, Nat. Methods 7 (2010) 989–994, https://doi.org/10.1038/nmeth.1532.

[54] P.J. Wrighton, J.R. Klim, B.A. Hernandez, C.H. Koonce, T.J. Kamp, L.L. Kiessling, Signals from the surface modulate differentiation of human pluripotent stem cells through glycosaminoglycans and integrins, Proc. Natl. Acad. Sci. U. S. A. 111 (2014) 18826–18131, https://doi.org/10.1073/PNAS.1409525111.

[55] R. Zufferey, D. Nagy, R.J. Mandel, L. Naldini, D. Trono, Multiply attenuated lentiviral vector achieves efficient gene delivery in vivo, Nat. Biotechnol. 15 (1997) 871–875, https://doi.org/10.1038/nbt0997-871.

[56] P. Salmon, D. Trono, Production and titration of lentiviral vectors, Curr Protoc Hum Genet 54 (2007), https://doi.org/10.1002/0471142905.hg1210s54.

[57] S. Satapathy, Provirus Silencing in Stem Cells: the Forbidden Regulators of Cell Fate, vol. 5, Sign Transduct Insights, 2016, https://doi.org/10.4137/STI.S12311. STI.S12311.

[58] Z. Ivics, P.B. Hackett, R.H. Plasterk, Z. Izsvák, Molecular reconstruction of sleeping beauty, a Tc1-like transposon from fish, and its transposition in human cells, Cell 91 (1997) 501–510, https://doi.org/10.1016/S0092-8674(00)80436-5.

[59] Z. Ivics, A. Katzer, E.E. Stüwe, D. Fiedler, S. Knespel, Z. Izsvák, Targeted sleeping beauty transposition in human cells, Mol. Ther. 15 (2007) 1137–1144, https://doi.org/10.1038/SJ.MT.6300169.

[60] L. Mátés, M.K.L. Chuah, E. Belay, B. Jerchow, N. Manoj, A. Acosta-Sanchez, D. P. Grzela, A. Schmitt, K. Becker, J. Matrai, L. Ma, E. Samara-Kuko, C. Gysemans, D. Pryputniewicz, C. Miskey, B. Fletcher, T. Vandendriessche, Z. Ivics, Z. Izsvák, Molecular evolution of a novel hyperactive Sleeping Beauty transposase enables robust stable gene transfer in vertebrates, Nat. Genet. 41 (2009) 753–761, https://doi.org/10.1038/ng.343, 2009 41:6.

[61] E. Kowarz, D. Löscher, R. Marschalek, Optimized Sleeping Beauty transposons rapidly generate stable transgenic cell lines, Biotechnol. J. 10 (2015) 647–653, https://doi.org/10.1002/BIOT.201400821.

[62] P.C. Fridy, Y. Li, S. Keegan, M.K. Thompson, I. Nudelman, J.F. Scheid, M. Oeffinger, M.C. Nussenzweig, D. Fenyö, B.T. Chait, M.P. Rout, A robust pipeline for rapid production of versatile nanobody repertoires, Nat. Methods 11 (2014) 1253, https://doi.org/10.1038/NMETH.3170.

[63] S. Konermann, P. Lotfy, N.J. Brideau, J. Oki, M.N. Shokhirev, P.D. Hsu, Transcriptome engineering with RNA-targeting type VI-D CRISPR effectors, Cell 173 (2018) 665–676.e14, https://doi.org/10.1016/J.CELL.2018.02.033.

[64] J.B. Black, S.R. McCutcheon, S. Dube, A. Barrera, T.S. Klann, G.A. Rice, S. S. Adkar, S.H. Soderling, T.E. Reddy, C.A. Gersbach, Master regulators and cofactors of human neuronal cell fate specification identified by CRISPR gene activation screens, Cell Rep. 33 (2020), 108460, https://doi.org/10.1016/J.CELREP.2020.108460.

[65] S. Hao, D. Baltimore, The stability of mRNA influences the temporal order of the induction of genes encoding inflammatory molecules, Nat. Immunol. 10 (2009) 281–288, https://doi.org/10.1038/ni.1699, 2009 10:3.

[66] J.M. Brunger, A. Zutshi, V.P. Willard, C.A. Gersbach, F. Guilak, Genome engineering of stem cells for autonomously regulated, closed-loop delivery of biologic drugs, Stem Cell Rep. 8 (2017) 1202–1213, https://doi.org/10.1016/J.STEMCR.2017.03.022.

[67] N. Farhang, J.M. Brunger, J.D. Stover, P.I. Thakore, B. Lawrence, F. Guilak, C. A. Gersbach, L.A. Setton, R.D. Bowles, CRISPR-based epigenome editing of cytokine receptors for the promotion of cell survival and tissue deposition in inflammatory environments, Tissue Eng. 23 (2017) 738–749, https://doi.org/10.1089/TEN.TEA.2016.0441.

[68] Y. Chen, J.Z. Shao, L.X. Xiang, X.J. Dong, G.R. Zhang, Mesenchymal stem cells: a promising candidate in regenerative medicine, Int. J. Biochem. Cell Biol. 40 (2008) 815–820, https://doi.org/10.1016/J.BIOCEL.2008.01.007.

[69] S. Aggarwal, M.F. Pittenger, Human mesenchymal stem cells modulate allogeneic immune cell responses, Blood 105 (2005) 1815–1822, https://doi.org/10.1182/BLOOD-2004-04-1559.

[70] Y. Han, X. Li, Y. Zhang, Y. Han, F. Chang, J. Ding, Mesenchymal stem cells for regenerative medicine, Cells 8 (2019) 886, https://doi.org/10.3390/cells8080886.

[71] D.I. Jang, A.H. Lee, H.Y. Shin, H.R. Song, J.H. Park, T.B. Kang, S.R. Lee, S. H. Yang, The role of tumor necrosis factor alpha (TNF-α) in autoimmune disease and current TNF-α inhibitors in therapeutics, Int. J. Mol. Sci. 22 (2021) 2719, https://doi.org/10.3390/IJMS22052719.

[72] V. Gerriets, A. Goyal, K. Khaddour, Tumor Necrosis Factor Inhibitors, StatPearls Publishing, 2022 (accessed June 26, 2022).

[73] M. Khoury, J. Adriaansen, M.J.B.M. Vervoordeldonk, D. Gould, Y. Chernajovsky, P. Bigey, C. Bloquel, D. Scherman, P.P. Tak, C. Jorgensen, F. Apparailly, Inflammation-inducible anti-TNF gene expression mediated by intra-articular injection of serotype 5 adeno-associated virus reduces arthritis, J. Gene Med. 9 (2007) 596–604, https://doi.org/10.1002/JGM.1053.

[74] L. Nissim, M.-R. Wu, E. Pery, A. Binder-Nissim, H.I. Suzuki, D. Stupp, C. Wehrspaun, Y. Tabach, P.A. Sharp, T.K. Lu, Synthetic RNA-based immunomodulatory gene circuits for cancer immunotherapy, Cell 171 (2017) 1138–1150, https://doi.org/10.1016/j.cell.2017.09.049.

[75] Y. Zhang, C. Pak, Y. Han, H. Ahlenius, Z. Zhang, S. Chanda, S. Marro, C. Patzke, C. Acuna, J. Covy, W. Xu, N. Yang, T. Danko, L. Chen, M. Wernig, T.C. Südhof, Rapid single-step induction of functional neurons from human pluripotent stem cells, Neuron 78 (2013) 785–798, https://doi.org/10.1016/j.neuron.2013.05.029.

[76] V. Busskamp, N.E. Lewis, P. Guye, A.H. Ng, S.L. Shipman, S.M. Byrne, N. E. Sanjana, J. Murn, Y. Li, S. Li, M. Stadler, R. Weiss, G.M. Church, Rapid neurogenesis through transcriptional activation in human stem cells, Mol. Syst. Biol. 10 (2014) 760, https://doi.org/10.15252/MSB.20145508.

[77] K.M. Hainline, L.S. Shores, N.L. Votaw, Z.J. Bernstein, S.H. Kelly, C.N. Fries, M. S. Madhira, C.A. Gilroy, A. Chilkoti, J.H. Collier, Modular complement assemblies for mitigating inflammatory conditions, Proc. Natl. Acad. Sci. U. S. A. 118 (2021), e2018627118, https://doi.org/10.1073/PNAS.2018627118.

[78] C. Yang, J. Dawulieti, K. Zhang, C. Cheng, Y. Zhao, H. Hu, M. Li, M. Zhang, L. Chen, K.W. Leong, D. Shao, An injectable antibiotic hydrogel that scavenges proinflammatory factors for the treatment of severe abdominal trauma, Adv. Funct. Mater. 32 (2022), 2111698, https://doi.org/10.1002/adfm.202111698.

[79] H. Shen, B. Xu, C. Yang, W. Xue, Z. You, X. Wu, D. Ma, D. Shao, K. Leong, J. Dai, A DAMP-scavenging, IL-10-releasing hydrogel promotes neural regeneration and motor function recovery after spinal cord injury, Biomaterials 280 (2022), 121279, https://doi.org/10.1016/J.BIOMATERIALS.2021.121279.

[80] H. Yin, Q. Lu, X. Wang, S. Majumdar, A.S. Jun, W.J. Stark, M.P. Grant, J. H. Elisseeff, Tissue-derived microparticles reduce inflammation and fibrosis in cornea wounds, Acta Biomater. 85 (2019) 192–202, https://doi.org/10.1016/J.ACTBIO.2018.12.027.

[81] S. Kumar, T. Conklin, J. Hsu, V. Meli, K. Chan, W. Liu, K. Allen, B. Sharma, Controlled release of CD200 inhibits inflammatory macrophages and chondrocyte catabolism, Osteoarthritis Cartilage 30 (2022), https://doi.org/10.1016/j.joca.2022.02.083. S69–S70.

[82] P.S. Briquez, H.M. Tsai, E.A. Watkins, J.A. Hubbell, Engineered bridge protein with dual affinity for bone morphogenetic protein-2 and collagen enhances bone regeneration for spinal fusion, Sci. Adv. 7 (2021) 4302–4313, https://doi.org/10.1126/SCIADV.ABH4302.

[83] N. Broguiere, I. Lüchtefeld, L. Trachsel, D. Mazunin, R. Rizzo, J.W. Bode, M. P. Lutolf, M. Zenobi-Wong, Morphogenesis guided by 3D patterning of growth factors in biological matrices, Adv. Mater. 32 (2020), https://doi.org/10.1002/ADMA.201908299.

[84] P. Camacho, A. Behre, M. Fainor, K.B. Seims, L.W. Chow, Spatial organization of biochemical cues in 3D-printed scaffolds to guide osteochondral tissue engineering, Biomater. Sci. (2021), https://doi.org/10.1039/D1BM00859E.

[85] C.A. DeForest, D.A. Tirrell, A photoreversible protein-patterning approach for guiding stem cell fate in three-dimensional gels, Nat. Mater. 14 (2015) 523–531, https://doi.org/10.1038/nmat4219.

[86] A.R. Martin, J.M. Patel, R.C. Locke, M.R. Eby, K.S. Saleh, M.D. Davidson, M. L. Sennett, H.M. Zlotnick, A.H. Chang, J.L. Carey, J.A. Burdick, R.L. Mauck, Nanofibrous hyaluronic acid scaffolds delivering TGF-β3 and SDF-1α for articular cartilage repair in a large animal model, Acta Biomater. 126 (2021) 170–182, https://doi.org/10.1016/J.ACTBIO.2021.03.013.

[87] G.S. Chendke, G. Faleo, C. Juang, A.v. Parent, D.A. Bernards, M. Hebrok, Q. Tang, T.A. Desai, Supporting survival of transplanted stem-cell-derived insulin-producing cells in an encapsulation device augmented with controlled release of amino acids, Adv Biosyst 3 (2019), 1900086, https://doi.org/10.1002/adbi.201900086.

[88] M.G. Burger, A. Grosso, P.S. Briquez, G.M.E. Born, A. Lunger, F. Schrenk, A. Todorov, V. Sacchi, J.A. Hubbell, D.J. Schaefer, A. Banfi, N. di Maggio, Robust coupling of angiogenesis and osteogenesis by VEGF-decorated matrices for bone regeneration, Acta Biomater. 149 (2022) 111–125, https://doi.org/10.1016/J.ACTBIO.2022.07.014.

[89] B.R. Freedman, A. Kuttler, N. Beckmann, S. Nam, D. Kent, M. Schuleit, F. Ramazani, N. Accart, A. Rock, J. Li, M. Kurz, A. Fisch, T. Ullrich, M.W. Hast, Y. Tinguely, E. Weber, D.J. Mooney, Enhanced tendon healing by a tough hydrogel with an adhesive side and high drug-loading capacity, Nat Biomed Eng (2022), https://doi.org/10.1038/s41551-021-00810-0.

[90] M.N. Barcellona, J.E. Speer, L. Jing, D.S. Patil, M.C. Gupta, J.M. Buchowski, L. A. Setton, Bioactive in situ crosslinkable polymer-peptide hydrogel for cell delivery to the intervertebral disc in a rat model, Acta Biomater. 131 (2021) 117–127, https://doi.org/10.1016/J.ACTBIO.2021.06.045.

[91] D.R. Hunt, K.C. Klett, S. Mascharak, H. Wang, D. Gong, J. Lou, X. Li, P.C. Cai, R. A. Suhar, J.Y. Co, B.L. LeSavage, A.A. Foster, Y. Guan, M.R. Amieva, G. Peltz, Y. Xia, C.J. Kuo, S.C. Heilshorn, Engineered matrices enable the culture of human patient-derived intestinal organoids, Adv. Sci. 8 (2021), 2004705, https://doi.org/10.1002/ADVS.202004705.

[92] R.S. Navarro, M.S. Huang, J.G. Roth, K.M. Hubka, C.M. Long, A. Enejder, S. C. Heilshorn, Tuning polymer hydrophilicity to regulate gel mechanics and encapsulated cell morphology, Adv Healthc Mater 11 (2022), 2200011, https://doi.org/10.1002/ADHM.202200011.

[93] V.v. Rao, M.E. Wechsler, E. Cravens, S.J. Wojda, A.S. Caldwell, B.E. Kirkpatrick, S.W. Donahue, K.S. Anseth, Granular PEG hydrogels mediate osteoporotic MSC clustering via N-cadherin influencing the pro-resorptive bias of their secretory profile, Acta Biomater. 145 (2022) 77–87, https://doi.org/10.1016/J.ACTBIO.2022.04.023.

[94] L.C. Ionescu, G.C. Lee, B.J. Sennett, J.A. Burdick, R.L. Mauck, An anisotropic nanofiber/microsphere composite with controlled release of biomolecules for fibrous tissue engineering, Biomaterials 31 (2010) 4113–4120, https://doi.org/10.1016/J.BIOMATERIALS.2010.01.098.

[95] C.R. Zamecnik, E.S. Levy, M.M. Lowe, B. Zirak, M.D. Rosenblum, T.A. Desai, An injectable cytokine trap for local treatment of autoimmune disease, Biomaterials 230 (2020), 119626, https://doi.org/10.1016/J.BIOMATERIALS.2019.119626.

[96] M.T. Wolf, S. Ganguly, T.L. Wang, C.W. Anderson, K. Sadtler, R. Narain, C. Cherry, A.J. Parrillo, B.v. Park, G. Wang, F. Pan, S. Sukumar, D.M. Pardoll, J. H. Elisseeff, A biologic scaffold-associated type 2 immune microenvironment inhibits tumor formation and synergizes with checkpoint immunotherapy, Sci. Transl. Med. 11 (2019) 7973, https://doi.org/10.1126/SCITRANSLMED. AAT7973.

[97] C. Gegg, F. Yang, Spatially patterned microribbon-based hydrogels induce zonally-organized cartilage regeneration by stem cells in 3D, Acta Biomater. 101 (2020) 196–205, https://doi.org/10.1016/J.ACTBIO.2019.10.025.

[98] K. Driscoll, M.S. Butani, K.A. Gultian, A. McSweeny, J.M. Patel, S.L. Vega, Plant tissue parenchyma and vascular bundles selectively regulate stem cell mechanosensing and differentiation, Cell. Mol. Bioeng. (2022) 1–12, https://doi.org/10.1007/S12195-022-00737-9.

[99] S.K. Bedingfield, J.M. Colazo, F. Yu, D.D. Liu, M.A. Jackson, L.E. Himmel, H. Cho, L.J. Crofford, K.A. Hasty, C.L. Duvall, Amelioration of post-traumatic osteoarthritis via nanoparticle depots delivering small interfering RNA to damaged cartilage, Nat Biomed Eng 5 (2021) 1069–1083, https://doi.org/10.1038/s41551-021-00780-3.

[100] E.B. Glass, A.A. Hoover, K.K. Bullock, M.Z. Madden, B.I. Reinfeld, W. Harris, D. Parker, D.H. Hufnagel, M.A. Crispens, D. Khabele, W.K. Rathmell, J. C. Rathmell, A.J. Wilson, T.D. Giorgio, F.E. Yull, Stimulating TAM-mediated anti-tumor immunity with mannose-decorated nanoparticles in ovarian cancer, BMC Cancer 22 (2022) 497, https://doi.org/10.1186/s12885-022-09612-2.

[101] N. Ortiz-Otero, J.R. Marshall, A. Glenn, J. Matloubieh, J. Joseph, D. M. Sahasrabudhe, E.M. Messing, M.R. King, TRAIL-coated leukocytes to kill circulating tumor cells in the flowing blood from prostate cancer patients, BMC Cancer 21 (2021) 1–12, https://doi.org/10.1186/S12885-021-08589-8.

[102] N. Aslankoohi, K. Mequanint, Intrinsically fluorescent bioactive glass-poly(ester amide) hybrid microparticles for dual drug delivery and bone repair, Mater. Sci. Eng. C 128 (2021), 112288, https://doi.org/10.1016/J.MSEC.2021.112288.

[103] E. Hopkins, E. Valois, A. Stull, K. Le, A.A. Pitenis, M.Z. Wilson, An optogenetic platform to dynamically control the stiffness of collagen hydrogels, ACS Biomater. Sci. Eng. 7 (2021) 408–414, https://doi.org/10.1021/acsbiomaterials.0c01488.

[104] S. Lenna, C. Bellotti, S. Duchi, E. Martella, M. Columbaro, B. Dozza, M. Ballestri, A. Guerrini, G. Sotgiu, T. Frisoni, L. Cevolani, G. Varchi, M. Ferrari, D.M. Donati, E. Lucarelli, Mesenchymal stromal cells mediated delivery of photoactive nanoparticles inhibits osteosarcoma growth in vitro and in a murine in vivo ectopic model, J. Exp. Clin. Cancer Res. 39 (2020) 1–15, https://doi.org/10.1186/S13046-020-01548-4.

[105] I. Batalov, K.R. Stevens, C.A. DeForest, Photopatterned biomolecule immobilization to guide three-dimensional cell fate in natural protein-based hydrogels, Proc. Natl. Acad. Sci. U. S. A. 118 (2021), e2014194118, https://doi.org/10.1073/PNAS.2014194118.

[106] C.S. Carson, K.W. Becker, K.M. Garland, H.M. Pagendarm, P.T. Stone, K. Arora, L. Wang-Bishop, J.J. Baljon, L.D. Cruz, S. Joyce, J.T. Wilson, A nanovaccine for enhancing cellular immunity via cytosolic co-delivery of antigen and polyIC RNA, J. Contr. Release 345 (2022) 354–370, https://doi.org/10.1016/J.JCONREL.2022.03.020.

[107] P.S. Lienemann, Q. Vallmajo-Martin, P. Papageorgiou, U. Blache, S. Metzger, A. S. Kiveliö, V. Milleret, A. Sala, S. Hoehnel, A. Roch, R. Reuten, M. Koch, O. Naveiras, F.E. Weber, W. Weber, M.P. Lutolf, M. Ehrbar, Smart hydrogels for the augmentation of bone regeneration by endogenous mesenchymal progenitor cell recruitment, Adv. Sci. 7 (2020), https://doi.org/10.1002/ADVS.201903395.

[108] G. Kelly, J.J. Milligan, E.M. Mastria, S. Kim, S.R. Zelenetz, J. Dobbins, L.Y. Cai, X. Li, S.K. Nair, A. Chilkoti, Intratumoral delivery of brachytherapy and immunotherapy by a thermally triggered polypeptide depot, J. Contr. Release 343 (2022) 267–276, https://doi.org/10.1016/J.JCONREL.2022.01.024.

[109] O.L. Lanier, J.M. Ficarrotta, I. Adjei, D. Wable, C. Lewis, C. Nacea, B. Sharma, J. Dobson, P. McFetridge, Magnetically responsive polymeric microparticles for the triggered delivery of a complex mixture of human placental proteins, Macromol. Biosci. 21 (2021), 2000249, https://doi.org/10.1002/mabi.202000249.

[110] S. Bhusari, S. Sankaran, A. del Campo, Regulating bacterial behavior within hydrogels of tunable viscoelasticity, Adv. Sci. 9 (2022), https://doi.org/10.1002/ADVS.202106026.

[111] A. Rodrigo-Navarro, S. Sankaran, M.J. Dalby, A. del Campo, M. Salmeron-Sanchez, Engineered living biomaterials, Nat. Rev. Mater. 6 (2021) 1175–1190, https://doi.org/10.1038/s41578-021-00350-8, 2021 6:12.

[112] T. Strittmatter, Y. Wang, A. Bertschi, L. Scheller, P.C. Freitag, P.G. Ray, P. Stuecheli, J.v. Schaefer, T. Reinberg, D. Tsakiris, A. Plückthun, H. Ye, M. Fussenegger, Programmable DARPin-based receptors for the detection of thrombotic markers, Nat. Chem. Biol. (2022), https://doi.org/10.1038/s41589-022-01095-3.

[113] D.J. Urban, B.L. Roth, DREADDs (designer receptors exclusively activated by designer drugs): chemogenetic tools with therapeutic utility, Annu. Rev. Pharmacol. Toxicol. 55 (2015) 399–417, https://doi.org/10.1146/annurev-pharmtox-010814-124803.

[114] B.L. Roth, DREADDs for neuroscientists, Neuron 89 (2016) 683–694, https://doi.org/10.1016/J.NEURON.2016.01.040.

[115] J.S. Park, B. Rhau, A. Hermann, K.A. McNally, C. Zhou, D. Gong, O.D. Weiner, B. R. Conklin, J. Onuffer, W.A. Lim, Synthetic control of mammalian-cell motility by engineering chemotaxis to an orthogonal bioinert chemical signal, Proc. Natl. Acad. Sci. U. S. A. 111 (2014) 5896–5901, https://doi.org/10.1073/PNAS.1402087111.

[116] K. Zohorsky, K. Mequanint, Designing biomaterials to modulate Notch signaling in tissue engineering and regenerative medicine, Tissue Eng. B Rev. 27 (2021) 383–410, https://doi.org/10.1089/TEN.TEB.2020.0182.

[117] A.B. Dietz, E.J. Dozois, J.G. Fletcher, G.W. Butler, D. Radel, A.L. Lightner, M. Dave, J. Friton, A. Nair, E.T. Camilleri, A. Dudakovic, A.J. van Wijnen, W. A. Faubion, Autologous mesenchymal stem cells, applied in a bioabsorbable matrix, for treatment of perianal fistulas in patients with crohn's disease, Gastroenterology 153 (2017) 59–62.e2, https://doi.org/10.1053/J.GASTRO.2017.04.001.

[118] C.H. Mosanya, J.D. Isaacs, Tolerising cellular therapies: what is their promise for autoimmune disease? Ann. Rheum. Dis. 78 (2019) 297–310, https://doi.org/10.1136/annrheumdis-2018-214024.

[119] J.M. Álvaro-Gracia, J.A. Jover, R. García-Vicuña, L. Carreño, A. Alonso, S. Marsal, F. Blanco, V.M. Martínez-Taboada, P. Taylor, C. Martín-Martín, O. DelaRosa, I. Tagarro, F. Díaz-González, Intravenous administration of expanded allogeneic adipose-derived mesenchymal stem cells in refractory rheumatoid arthritis (Cx611): results of a multicentre, dose escalation, randomised, single-blind, placebo-controlled phase Ib/IIa clinical trial, Ann. Rheum. Dis. 76 (2017) 196–202, https://doi.org/10.1136/annrheumdis-2015-208918.

[120] N. Fujiwara, J. Shimizu, K. Takai, N. Arimitsu, A. Saito, T. Kono, T. Umehara, Y. Ueda, S. Wakisaka, T. Suzuki, N. Suzuki, Restoration of spatial memory dysfunction of human APP transgenic mice by transplantation of neuronal precursors derived from human iPS cells, Neurosci. Lett. 557 (2013) 129–134, https://doi.org/10.1016/J.NEULET.2013.10.043.

[121] V. Vasic, K. Barth, M.H.H. Schmidt, Neurodegeneration and neuro-regeneration—alzheimer's disease and stem cell therapy, Int. J. Mol. Sci. 20 (2019) 4272, https://doi.org/10.3390/ijms20174272.